The Cumulative Impact of Cloud Droplet Nucleating Aerosols on Orographic Snowfall in Colorado

STEPHEN M. SALEEBY*

Colorado State University
Ft. Collins, Colorado

WILLIAM R. COTTON

Colorado State University
Ft. Collins, Colorado

JAMIE D. FULLER

Colorado State University
Ft. Collins, Colorado

Revised for publication in Journal of Applied Meteorology and Climatology
October 27, 2010

Corresponding author address: Stephen M. Saleeby, Colorado State University, Atmospheric Science Department, Fort Collins, CO 80523. e-mail: smsaleeb@atmos.colostate.edu

Abstract

Hygroscopic pollution aerosols have the potential to alter winter orographic snowfall totals and spatial distributions by modification of high elevation supercooled orographic clouds and the riming process. We investigate the cumulative effect of varying the concentrations of hygroscopic aerosols during January-February for four recent winter snowfall seasons over the high terrain of Colorado. The Regional Atmospheric Modeling System (RAMS) version 6.0 is used to determine the particular mountain ranges and seasonal conditions that are most susceptible. Multiple winter seasonal simulations are run at both 3km and 1km horizontal grid spacing with varying aerosol vertical profiles. Model predicted snowfall accumulation trends are compared to automated snow water equivalent observations at high elevation sites.

An increase in aerosol concentration leads to reduced riming of cloud water by ice particles within supercooled, liquid orographic clouds, thus, leading to lighter rimed hydrometers with slower fall speeds and longer horizontal trajectories. This effect results in a spillover of snowfall from the windward slope to the lee ward slope. A snowfall spillover effect is most evident in the southern and western region of the San Juan Range where high moisture-laden storms are more prevalent. The effect over the Park Range is also present in each simulated season, but with lower amplitudes and slightly varying magnitudes among seasons. Seasons with greater overall snowfall exhibit a greater response in magnitude and percentage change. The smallest spillover effect occurred downwind of the primary western slope mountain barriers.

While the aerosol effect on snowfall can be locally significant in particularly wet winter seasons, the inter-seasonal variability in synoptic conditions can impose much larger, widespread changes in snowfall accumulation.

1. Introduction

The orography of a mountainous region exerts a dramatic influence on the development of clouds and precipitation and leads to local enhancements in precipitation (Fraser et al. 1973; Hobbs et al. 1973; Rauber and Grant 1986). Upslope flow conditions and sufficient moisture lead to parcel supersaturation, ice crystal nucleation and growth, and formation of supercooled orographic clouds (Rauber and Grant 1986; Borys et al. 2000; Saleeby et al. 2009). The amount and spatial distribution of orographic precipitation depends upon a number of factors, including the geometry of the terrain, background flow dynamics, atmospheric stability, and cloud microphysics (e.g., Fraser et al. 1973; Hobbs et al. 1973; Colle 2004; Colle et al. 2005, 2008; Rutunno and Houze 2007, Saleeby et al. 2007, Muhlbauer and Lohmann 2008). The annual precipitation in Colorado is dominated by orographic snowfall during the winter months (Borys and Wetzel 1997). Observational and modeling studies have shown that, on average, snowfall amount and local terrain height variability are strongly positively correlated (Wetzel et al. 2004; Saleeby et al. 2009), such that the highest, steepest mountain ridges tend to accumulate the greatest snowfall totals. Given the high elevation of Colorado topography, the vast majority of wintertime snow and liquid water clouds have temperatures well below freezing, and thus, hydrometeor growth evolution is controlled by cold cloud processes (Hindman 1986).

The greatest wintertime precipitation efficiency occurs when vapor depositional growth of snow crystals and accretion of supercooled liquid water droplets are optimal. The accretion growth of snow crystals by collection of supercooled cloud droplets, known as riming, occurs as the crystals assume trajectories that pass through an orographic cloud. If both snow and supercooled liquid water clouds co-exist, the riming process can lead to collection of a substantial amount of cloud water in the lowest 2km of the orographic cloud, where liquid water

contents are highest (Rauber and Grant 1986; Reinking et al. 2000; Saleeby et al. 2009). This effect has been observed to enhance surface precipitation amounts by up to 20-50% near mountaintop (Mitchell 1990; Borys et al. 2003). An observational study of high elevation sites in Colorado, by Hindman (1986), revealed that supercooled liquid water clouds and rimed snow were most abundant along primary mountain barriers such as Wolf Creek Pass in the southwestern San Juan Range and Steamboat Springs in the northern Park Range. Secondary ranges that are typically blocked by the primary ranges may succumb to subsidence from the primary ranges or a reduction in available moisture that was precipitated upwind.

The amount of riming growth of an individual snow crystal is a function of the trajectory through the cloud, the cloud liquid water content (LWC), cloud droplet number concentration (CDNC), cloud droplet sizes, and snow crystal size and habit (Hindman 1986; Hindman et al. 1992; Borys et al. 2000; Saleeby et al. 2009). From observations of supercooled liquid water clouds, it was concluded that riming is reduced as droplet sizes decrease due to a reduction in the collision efficiency between snow crystals and small droplets (Hindman et al. 1992; Borys et al. 2000; Borys et al. 2003). As droplet size decreases there is less mass for efficient inertial impaction and a greater fraction of droplets flow around a crystal. Below about 10 μm diameter the riming efficiency of droplets rapidly approaches zero (Pitter and Pruppacher 1974; Wang and Ji 2000).

The introduction of high concentrations of hygroscopic pollution aerosols into an orographic cloud has the potential to dramatically alter the cloud droplet spectra through the nucleation of additional cloud droplets, with subsequently, smaller mean diameters and smaller riming efficiency. At the high altitude Storm Peak Laboratory (SPL) in Steamboat Springs, Colorado, Borys et al. (2000,2003) observed a direct relationship between sulfate concentration

and CDNC and an inverse relationship between sulfate concentration and: droplet size, rimed mass fraction, and snowfall rate. They established that sulfate concentration is a reliable proxy for hygroscopic aerosol number concentration. Statistical climatology studies of observed precipitation differences due to the aerosol second indirect effect were performed by Givati and Rosenfeld (2004), Jirak and Cotton (2006), and Rosenfeld and Givati (2006). The second indirect effect involves a decrease in precipitation by aerosols via an increase of CDNC, a consequent decrease in mean droplet size (for a given liquid water content), and slower onset of collision coalescence (for warm clouds) or less efficient riming (for mixed phase clouds) (Albrecht 1989). These studies showed a decrease over time in precipitation downwind of highly polluted urban areas and no change in precipitation downwind of rural areas. Givati and Rosenfeld (2004) introduced the orographic enhancement factor, which is the ratio of upwind precipitation to that measured at a downwind high elevation mountain site. In polluted regions, they found the orographic enhancement to be reduced over time, while in remote regions there was no change.

Recent numerical modeling studies have also addressed the impacts of aerosols on orographic precipitation. Saleeby et al. (2009) performed high resolution modeling experiments, centered over SPL, in which they varied the aerosol vertical profiles, from clean to polluted, for particular snowfall events in 2007 that were dominated by cold cloud processes. Additional aerosols led to more numerous, smaller cloud droplets, reduced riming and graupel mass, and a shift in precipitation from the windward to leeward slope. Given the quasi-stationary nature of these winter orographic clouds, the additional aerosols did not lead to substantially higher cloud tops or greater liquid water path as might be expected from clouds systems where latent heat release is a greater driving force (Khain et al. 2004, 2005). Though the precipitation spillover effect was impressive, there was an insignificant net total precipitation change across the affected

region. Precipitation particles were primarily redistributed from heavily rimed, faster-falling graupel particles to unrimed or lightly rimed, slower-falling snow crystals and aggregates of crystals, with aggregates becoming the most abundant hydrometeor species.

In comparison, Lynn et al. (2007) performed numerical simulations over the Sierra Nevada mountain range using a binned-resolving microphysics model. Their simulations contained stronger updrafts, convective elements, and a variable mixture of warm and cold cloud processes. In general, an increase in aerosols from a maritime airmass to a continental airmass led to a downwind shift in precipitation, reduced amounts of rain and graupel, and an overall precipitation reduction across the domain. The maritime aerosol concentration resulted in rain and graupel production and accumulation on windward slopes, while the increase to continental aerosol concentrations produced stronger updrafts, higher cloud tops, suppressed warm rain process, and greater ice production via enhanced glaciation. Stronger leeward subsidence and evaporation in the continental case partially provided the mechanism for total precipitation reduction.

In purely warm-phase orographic precipitation simulations, Muhlbauer and Lohmann (2008) reveal a total rainfall reduction as well as a downstream shift in the rainfall maximum for increased aerosol loading. This effect is primarily attributed to suppression of the cloud droplet autoconversion process. They also note that this microphysical response is most prevalent for narrow mountain ranges in an unblocked flow environment. The downstream shift in precipitation becomes progressively closer to the mountain ridge as the mountain width is increased. In a follow-on study of idealized mixed-phase orographic clouds and precipitation, Mulhbauer and Lohmann (2009) found that higher concentrations of internally mixed aerosols will reduce the warm-rain formation process, the riming rate, and the accumulated precipitation.

However, the amount of precipitation reduction will vary depending on the environmental thermodynamic profile as well as the relative contributions to precipitation from riming of cloud water by small ice crystals and aggregation of small nucleated ice crystals. In warmer conditions, the aggregation collection efficiency is higher. As such, if aggregation is the dominant precipitating hydrometeor formation mechanism, then aerosol effects may be minimized since the amount of total riming growth would be small compared to aggregation growth. The ability to adequately model the effects of riming is crucial for determining the impacts of aerosols on mixed-phase or cold phase precipitation. Hence, both Lohmann (2004) and Saleeby and Cotton (2008) introduce riming schemes that are based on size-dependent collection kernels, and which lead to reduced riming rates compared to models that use a single hydrometeor distribution mass-weighted riming efficiency. These model improvements provide more realistic riming rates which may lead to more realistic interpretations of model microphysical responses to aerosol loading where riming is a dominant precipitation process.

Modifications to the amount and distribution of orographic precipitation can have great implications on regional hydrology and water resources (Smith et al. 2005; Saleeby et al. 2009). As such, this modeling study seeks to expand upon the work of Saleeby et al. (2009), which focused on observing and modeling the impact of aerosols over the north-central Park Range of Colorado for short period winter weather events that occurred during a field study at SPL in January and February 2007. Here we will examine the cumulative effect of increasing the concentration of hygroscopic aerosols over the entire Colorado Rocky Mountains for the months of January and February in 2005, 2006, 2007 and 2008. We chose to simulate these four consecutive seasons since they encompass a range of seasonal conditions and snowfall totals and include the 2005 and 2007 seasons, in which case study simulations were evaluated by Saleeby

et al. (2006, 2007, 2009). From an ensemble of simulations we investigate the following questions:

- Are there particular mountain ranges in Colorado where snowfall is more susceptible to increases in aerosol concentration?
- Does the precipitation spillover effect occur from infrequent events, or is this effect common throughout the winter season?
- Is there inter-seasonal variability in the impact of aerosols on precipitation modification, and how does this relate to total seasonal snowfall and persistence of orographic supercooled liquid water clouds?
- How does the cumulative precipitation response to aerosols impact the regional hydrology of Colorado with respect to the various river basins and watersheds?

2. Numerical model

This modeling study is performed using the Colorado State University (CSU) Regional Atmospheric Modeling System (RAMS) version 6.0. RAMS is run as a non-hydrostatic, fully compressible model on an Arakawa-C grid and sigma-z terrain following coordinate system with two-way nested feedback (Cotton et al. 2003). In the simulations for this study, we initially employ the following nested three grid arrangement: grid 1 covers much of the United States at 36-km grid spacing (85 x 75 grid points), grid 2 covers Colorado and portions of the adjacent states at 12-km grid spacing (68 x 68 grid points), and grid 3 covers most of Colorado, except a portion of the eastern plains, at 3-km grid spacing (146 x 150 grid points) (Fig 1). Within each grid there are 38 vertical levels with minimum 75m vertical grid spacing. We use vertical grid stretching with a stretch ratio of 1.12 and maximum grid spacing of 750m. The 32km North

American Regional Reanalysis (NARR) (Mesinger et al. 2006) was used for model initialization and boundary nudging of the geopotential height, temperature, relative humidity, and winds on grid-1, and the radiative boundary condition of Klemp and Wilhelmson (1978) was applied to the lateral boundaries. The model extends sufficiently high into the stratospheric so as to allow for gravity wave damping and prevention of wave reflection off of the model top. RAMS used the hydrometeor-sensitive radiation scheme of Harrington (1997), the Land Ecosystem-Atmosphere Feedback-2 surface flux model (Walko et al. 2000), the horizontal turbulent diffusion of Smagorinsky (1963), and the vertical turbulent kinetic energy level-2.5 closure of Mellor and Yamada (1974). The Kain and Fritsch (1993) cumulus parameterization was applied to grids 1 and 2, while convection was resolved explicitly on grid 3. While there would be inherent variability among simulations using various model parameterizations of microphysics, land surface, radiation, and the boundary layer, the current combination of parameterizations is based on that used by Saleeby et al. (2009), which resulted in realistic high-resolution, short-term snowfall simulations for case studies over the Park Range and a defined aerosol effect on snowfall distribution.

Simulations used a bin-emulating, two-moment, bulk microphysics module that prognoses mixing ratio and number concentration of cloud droplets, rain, pristine ice, snow, aggregates, graupel, and hail (Walko et al. 1995; Meyers et al. 1997). Hydrometeors are represented by gamma distributions with defined shape parameters (Walko et al. 1995). The cloud droplet distribution uses a gamma function shape parameter of $\nu=4$, and all other hydrometeor categories use $\nu=2$. A value of $\nu=1$ would represent a Marshall-Palmer distribution, and higher values of ν give narrower distributions. Changes in the cloud droplet distribution shape parameter for varying widths of the gamma distribution would likely have only a modest

influence on the aerosol effects on snowfall. Broadening the distribution would rearrange the cloud droplet number across a larger size range, which, generally, accelerates droplet autoconversion, in warm rain situations, but not necessarily the riming process. Other tunable microphysical parameters, such as hydrometeor fall speeds, aggregation efficiency, and ice crystal habits may also impact resulting snowfall and aerosol influences. With this in mind, it was chosen for this study to hold such variables constant at reasonable values and examine the microphysical response to a change in aerosol concentration.

The cloud droplet nucleation scheme activates a percentage of the aerosol population based on the environmental temperature, vertical velocity, hygroscopic aerosol concentration, and aerosol log-normal distribution median radius according to the methodology of Saleeby and Cotton (2004). This method uses a lookup table approach that is based on Lagrangian parcel model simulations that relate vertical velocity to supersaturation and subsequent aerosol activation via the Kohler equations (Heymsfield and Sabin 1989). Aerosols are assumed to be ammonium sulfate, which is a reasonable estimate, given the sulfate analyses by Borys et al. (2000, 2003) of snow and rime ice from SPL.

Primary heterogeneous ice nucleation is based on the Meyers formula (Meyers et al. 1997), and uses a density weighted vertically decaying profile with height with a maximum ice nuclei number concentration of 100 L^{-1}. Contact ice nucleation, homogeneous freezing of droplets, haze droplet nucleation, and secondary ice production [ice splintering via Mossop (1976)] are also represented. We employ the binned riming approach from Saleeby and Cotton (2008) that utilizes size dependent collection efficiencies between ice particles and cloud droplets from Wang and Ji (2000), Cober and List (1993), and Greenan and List (1995).

When riming occurs in the microphysics model between snow and cloud water, the new internal energy of the snow category is computed for the combination of frozen and rimed liquid condensate. During light riming, the internal energy may be raised only slightly, and the snow remains completely frozen. In this case all of the combined mass of snow and rimed cloud water stays in the snow category. This would represent snow crystals that retain their distinct habit and shape in spite of riming. This may affect the size of the snow crystals slightly, which may impact the fall speeds that are based on power laws related to mean diameter. If heavier riming occurs and the internal energy of the snow category raises enough to determine that the rimed cloud water leaves a liquid layer, then the higher energy liquid mass (part cloud water and part snow) is transferred to the graupel category. This category can represent a mixture of ice and liquid, and has a higher density and fall speed than snow. This partitioning of ice hydrometeors between unrimed or lightly rimed snow and more heavily rimed ice particles (graupel) is the microphysical pathway leading to the spillover effect of wintertime mixed-phase precipitation.

For each of the 60-day simulations beginning January 1 of 2005, 2006, 2007, and 2008, horizontally homogeneous, vertically decreasing aerosol concentration profiles were imposed per Saleeby et al. (2009) and Storer et al. (2010). The aerosol concentration represented here is a population of unactivated hygroscopic aerosols that fit a log-normal distribution with median radius of 0.04 μm. The percentage of aerosols that activate and lead to droplet nucleation is partly based on the vertical velocity, which is a proxy for supersaturation as determined from the parcel model simulations previously mentioned. A set of simulations were run for each season with clean (CL), moderately polluted (MP), and highly polluted (HP) aerosol profiles with respective maximum surface concentration of 100, 800, and 1500 cm^{-3}. The aerosol concentration decreases linearly with height up to 4.0km AGL and is then set to a background

concentration of 100 cm^{-3} above. The clean aerosol simulations represent the control runs for each season, and as such, several of the figures discussed below will present results from only control simulations. Changes due to aerosol perturbations will be displayed in separate figures.

Given the lengthy duration of the simulations and the inherent difficulty in applying realistic aerosol source functions, the aerosol profiles remained constant throughout the simulations. During the cloud nucleation process, a given grid point cannot activate more aerosols than allowed by the predicted ambient conditions, including vertical velocity (supersaturation), at that location. For example, if a cloud-free grid cell has an aerosol concentration of 1000 cm^{-3}, and the ambient conditions, including vertical velocity, lead to a nucleation-lookup-table value of 45%, then 450 cm^{-3} aerosols activate and lead to formation of 450 cm^{-3} cloud droplets in that grid cell. To nucleate additional droplets, the vertical velocity (supersaturation) would need to increase and lead to a look-up table value higher than the initial 45%. A given grid cell will only support a cloud droplet population representative of the supersaturation and other ambient conditions as determined from the parcel model generated nucleation look-up tables.

Given available computational resources, each 60-day simulation, nested down to 3km grid spacing, required 15 days of wall clock time for completion. For a sum of 12 simulations, total compute time required 180 days. While we would have preferred to perform simulations at finer grid-spacing, the duration of the simulations and total compute time were inherently prohibitive. However, additional simulations at finer grid spacing were performed for a shorter duration to examine the sensitivity of modeling the aerosol effects to a change in resolution. From these initial simulations it will be shown that the 2005 season produced the greatest snowfall totals and greatest sensitivity to changes in aerosol concentration with respect to total

precipitation modification. As a follow up study, three simulations were performed for January 2005 at 1km grid spacing over the San Juan Mountains in the southwestern corner of Colorado. This region was chosen since it proved to exhibit the greatest sensitivity to changes in aerosol concentration. Results of the initial "seasonal" sensitivity simulations are discussed below, followed by the results of the comparison between the 3km and 1km grid spacing simulations. The analyses shown, hereafter, focus solely on the finest resolution grids in which microphysical processes generate precipitation and the convective parameterization is inactive.

3. Results

a. Total Precipitation

Total accumulated snowfall, represented as snow water equivalent (SWE), for the clean seasonal simulations is shown in figure 2. This figure also contains markers for several automated SNOw TELemetry (SNOTEL) sites across the domain that will be referenced below. Several key mountainous areas that will be emphasized in the following sections are marked in the bottom panel of figure 1. These are the (1) Park Range, (2) Summit County Region, (3) Flat Tops, (4) San Juan Range, (5) Grand Mesa, and (6) Uncompahgre Plateau.

The winter seasons of 2005 and 2008 exhibit the greatest precipitation totals among the four seasons, with 2005 having the greatest overall precipitation coverage across the state. Of the drier 2006 and 2007 seasons, 2006 received the least snowfall in terms of both magnitude and spatial coverage. When comparing the 2005 and 2008 seasons, there is a noticeable difference in snowfall maxima. The 2005 simulation produces greater snowfall in the San Juan Range of southwest Colorado than in 2008. In 2008, there is more snow accumulated in the northern half of the domain including the Park Range, Flattops, and northern Front Range than in 2005.

Snowfall amounts in the central mountains are very comparable in 2005 and 2008. This suggests that in 2005 the winter storm tracks led to predominantly southwesterly flow, and in 2008 the flow was primarily westerly to northerly.

Figures 3-5 display the January-February 60-day mean fields of the 500mb geopotential heights, 500mb geopotential height anomalies, and 700mb relative humidity anomalies from the NARR dataset, respectively, for each season. The 60-day mean anomalies are computed as the average of the daily anomaly fields, which are computed by subtracting the long term daily mean (1979-2007) from the daily mean for each day. The 500mb geopotential height fields display similar northwesterly flow conditions over Colorado in 2006, 2007, and 2008, though heights are lower over Colorado and the northwest U.S. during 2008. The flow in 2005 differs from the other seasons, with more zonal flow over Colorado and southwesterly flow over the southwest U.S. in association with an averaged trough condition just offshore of southern California. From the geopotential height anomaly field there is a greater persistence in 2005 for low pressure systems over the southwest U.S. There is a lower pressure pattern and predominantly northwesterly flow in 2008, mostly neutral or average conditions in 2007, and an above normal height anomaly over the southwest U.S. in 2006. From the relative humidity fields, it was exceptionally moist in 2005, slightly moist in 2008, neutral in 2007, and drier over Colorado and the southwest U.S. in 2006. The mean height field and moisture patterns support the tendency for heavy snowfall in 2005 (greatest in southwest CO) and 2008 (greatest in northern CO), as well as the lower snowfall totals in 2006 and 2007. It will become evident from the following discussion and figures, that while the aerosol impact on snowfall is important from a human impacts perspective, the interseasonal variability in precipitation due to variable synoptic conditions can far exceed the impact of pollution aerosols.

b.SNOTEL Observations

While all numerical weather prediction models have their limits of predictability, Wetzel et al. (2004), Saleeby et al. (2005, 2006, 2007, 2009), and Saleeby and Cotton (2008) have demonstrated that the CSU-RAMS model performs rather well in winter snowfall prediction for individual cases over the Park Range with a tendency for over-prediction in some individual events. Expansion of model simulations toward seasonal scales and coverage over the whole of Colorado reveal a range of variability in prediction that varies among seasons, individual events, and in location across the domain. Time series of SWE, measured with a snow pillow, from the SNOTEL sites identified in figure 2 provide a comparison to simulated snowfall (figure 6). In figure 6 the simulated time series of SWE from the corresponding grid point closest to the SNOTEL locations are shown. Also shown are the time series for locations two grid points down-slope of the SNOTEL point. The down-slope point time series are displayed so as to demonstrate the strong gradient in simulated precipitation along the steep topography in the regions near the high elevation SNOTEL sites.

In terms of variability among seasons, the SNOTEL observation sites of Sharkstooth (SKZ) and Wolf Creek Summit (WLF) in the San Juan Range receive the greatest snowfall in 2005 and 2008, with 2005 being slightly greater under predominant southwesterly flow. The total values in 2006 and 2007 are substantially less, with 2006 being the driest. The central SNOTEL locations of Overland Reservoir (OVR) and Columbine Pass (COP) also receive greater snowfall in 2005 and 2008. Rabbit Ears Pass (RAB) and Joe Wright Reservoir (JOE) receive more snowfall in 2008 than in 2005, which follows from the predominant northwesterly flow in 2008 and southwesterly flow in 2005.

Comparisons between the SNOTEL and RAMS time series generally reveal an over-prediction of snowfall for the SNOTEL grid point locations (figure 6). The amount of over-prediction varies among location and season. In some cases, the SNOTEL time series falls below the model closest grid point time series and that of the down-slope grid point, while in other cases the SNOTEL time series falls between the two. The over-prediction by the model likely is a result of the combined effect of model grid spacing and terrain representation. While we wanted to represent terrain height most accurately, a more abrupt terrain change between grid cells may be leading to over-predicted convergence along the sigma-Z terrain following coordinate system. In the case of coarser grid spacing, it may be more appropriate to smooth the terrain representation to limit large differences in elevation between adjacent grid cells. While keeping in mind the challenges of quantitative precipitation prediction and the variability and biases in simulated snowfall, we can examine aerosol impacts on snowfall magnitudes and spatial distribution.

c. Aerosol-induced precipitation change

The total 60-day accumulated precipitation differences due to the increase in maximum aerosol concentrations from 100 to 1500 cm^{-3} are show in figure 7. From a broad perspective, the variability in magnitude and spatial extent of the precipitation modification due to aerosol loading follows the variability in total precipitation seen in figure 2. This means that the magnitude and area impacted by aerosol variability increases as the total seasonal snowfall amounts increase. As such, the 2005 winter season displays the greatest sensitivity to increasing aerosol concentration with respect to total changes in local snowfall amounts. The 2006 season

experiences only minor snowfall modifications, with very few localized areas exceeding a snowfall change greater than 5mm SWE over 60 days.

Upon examination of the patterns in snowfall change in 2005, it becomes apparent that there are numerous snowfall modification couplets that are coincident with the highest mountain ranges and steepest topography. The regions of reduced snowfall are primarily located on the windward slopes and enhanced snowfall appears on the leeward slopes. This pattern is indicative of the spillover effect discussed in Saleeby et al. (2009). This pattern is caused by a reduction in snow crystal riming, which allows snow to retain a low hydrometeor density with small fall speeds and long horizontal advection trajectories; this promotes surface deposition on downwind terrain in polluted conditions. The most dominant snowfall change couplets occur in the regions marked by the SNOTEL site markers on figure 7. The San Juan mountain range, indicated by WLF and SKZ, contains the largest, most continuous couplet in 2005. The San Juan range is also the largest and highest mountain range in Colorado, boasting roughly 1/3 of the 54 Colorado peaks that exceed 14,000 feet in elevation. This region, along with the Park Range, even experiences a small spillover effect in the driest winter (2006). The interior or eastern mountains, including the Summit County region experience less of a spillover effect due to aerosols; this would tend to agree with the hypothesis of Hindman (1986), which postulates that the formation of orographic supercooled liquid water clouds may be inhibited in regions downwind of primary mountain barriers due to a combination of subsidence drying and upstream moisture removal by primary barriers. This effect appears most prominent in the 2008 season in which the spillover effect is generally confined to the primary upstream mountain ranges.

Table 1 displays the bulk magnitude changes in precipitation over Colorado due to increasing aerosol concentration. Column 1 indicates the simulation year and the representative

change in aerosols. In columns 2-4 we examine the percentage change in the domain-summed volume of SWE that accumulates over the 60-day period for each season and for the increases in pollution aerosols from CL to MP, MP to HP, and CL to HP. Generally, there is a modest decrease in total net SWE for increases in aerosol concentration. Even the heaviest snowfall season of 2005 experiences only a maximum net decrease of about -1.5%.

In columns 3-6, the reported increase (decrease) in SWE is the change in SWE summed over all grid cells that experience an increase (decrease) in SWE. When the change in SWE volume is delineated between grid cells with a net increase or net decrease (column 3,4) we see that the total SWE volume in grid cells that experience a decrease is a maximum of -2.96% in 2005, and the total increase is a maximum of 1.48% in 2005 as well; seasons with less precipitation experience a smaller percentage change. The spillover effect does not completely compensate for the loss of windward slope precipitation. Upon closer examination, the decreases or increases in SWE are proportionally greater in the initial increase in aerosol concentration from CL to MP than in the subsequent step up from MP to HP; a *highly polluted* environment is not a necessary requirement for modification of the riming process. Next we examine the percent change in the area impacted by aerosol loading. Columns 5-6 display the percentage of the domain area that experienced a decrease or increase in accumulate SWE of at least 5mm at the end of 60 days of simulation time. The 2005 season encounters the greatest widespread changes in SWE, with approximately 32% (21%) of the domain experiencing a snowfall loss (gain) when aerosol concentration is increased from CL to MP. Maximum grid point changes in SWE, seen in columns 7 and 8, are highest in the heavy snowfall seasons, and they show greater changes when increasing aerosols from CL to MP rather than MP to HP. Furthermore, the maximum grid point

decrease in SWE tends to be greater than the maximum increase for the majority of seasons and changes in aerosol concentration.

The time series of SWE from the CL simulation in 2005 and change in SWE due to increasing aerosol concentration from CL to HP are plotted in figure 8 from the grid point with maximum snowfall loss. Also plotted are the time series of the maximum local gain in SWE, located just downstream of the point with maximum loss, as well as the point between the maximum loss and gain where the change in SWE is nearly neutral. These three points are identified, respectively, as "Maximum Loss Point", "Relative Gain Point", and "Near Neutral Point". The neutral point is located near the ridgeline where there is an approximate even balance between loss of heavily rimed ice hydrometeors and gain of unrimed or lightly rimed snow. From the overall accumulation of SWE it is seen that the snowfall is rather continuous and heavy from Jan 1-12 for each of the points, with the greatest snowfall at the neutral point located along the ridgetop. The lee slope grid point receives the least snowfall of these three points. From Jan 12-27 there is no snowfall at these locations. From Jan 27 to the end of the simulations on Mar 1, the snowfall increases over time with periodic steps in accumulation in association with passage of large scale synoptic winter weather events.

Panel b of figure 8 displays the modeled change in SWE over time in 2005 due to high aerosol loading for each of the points described above. The maximum loss point displays a trend that generally follows the accumulation trend with periodic steps in accumulation change. However, a closer comparison reveals that some of the accumulation events do not lead to a SWE loss, while others lead to a substantial loss. This implies that not every snowfall event at these high elevations is accompanied by a supercooled orographic liquid water cloud. Increases in snowfall at the relative gain grid point coincide with decreases at the maximum loss grid

point; though, the magnitude of the lee slope increase is consistently less than the upstream loss. The time series representing the point of near zero net change in SWE displays some fluctuation over time; it contains periods of snowfall enhancement and suppression that balance out over time. This suggests that the horizontal impact of the aerosol spillover effect can vary with each given snowfall event. Saleeby et al. (2007) discussed a model study that showed a strong correspondence between wind speed and the horizontal distribution of snowfall. Stronger wind speeds in the lowest few kilometers above the surface led to a downstream displacement in maximum orographic snowfall and in the aerosol-induced spillover effect. As such, a reduction in snowfall at the net-zero point would indicate an event with stronger horizontal flow, and vice versa. It is also possible that variability in wind direction among snowfall events may modify the snowfall spatial distribution relative to the ridgeline.

d. Cloud droplet number concentration

The change in accumulated precipitation is ultimately a result of changes in cloud droplet number concentration and cloud droplet size. For the same cloud water content, and increase in cloud droplet number, due to higher aerosol concentrations, leads to smaller droplets with lower riming efficiencies. Figure 9 displays time series points of domain averaged cloud droplet number concentration every three hours for the 60 days of simulation time for each simulated season. The time series points are plotted for the CL (red diamonds), MP (blue squares), and HP (black triangles) aerosol sensitivity simulations. Also plotted, in black contours, is the time series indicating the percentage of the domain grid cells below 10km AGL that contain cloud water greater than 0.05 g kg^{-1}. This trace was included to indicate the relative sample volumes used for computing average droplet concentration; the domain cloudiness trace was only shown from the

CL simulations since there was little variability in this quantity due to changes in aerosol. The cloud water threshold was also applied to grid cells included in the domain average of cloud droplet number concentration.

Average droplet concentrations varied substantially over time for the CL, MP, and HP simulations and for each season simulated. This is indicative of the variability in supersaturation across the Colorado domain. The CL aerosol simulation leads to average droplet concentrations that vary from near zero to a maximum of 100 cm^{-3}. Much of the time, though, values are in the 30-80 cm^{-3} range, which is representative of clean cloud conditions at a high elevation site indicated by Borys et al. (2000, 2002, 2003). The MP simulations with maximum aerosol concentration of 800 cm^{-3} frequently led to droplet concentrations in the range of 200-500 cm^{-3}; these values would fall within the range of observed polluted conditions at SPL as indicated by Borys et al. (2000, 2002, 2003). The HP simulations led to a wide range of average droplet concentrations with values often clustered in the range of 500-800 cm^{-3}. While this is in excess of most of the limited wintertime observations in Colorado it is certainly not out of the realm of possibility during periods of aerosol intrusion.

e. Cloud and ice water path

Figure 10 displays plots of the time averaged cloud liquid water path (CWP) for the duration of the 60-day clean simulations. During simulation runtime, model results were output every three hours for the full 60-days. The results for figure 10 were obtained by averaging CWP at three hourly intervals. Similar to the total precipitation fields, the total CWP is greatest for the 2005 and 2008 seasons, and it is substantially less in 2006 and 2007. The regions with the greatest spillover effect (fig 7) coincide with regions of highest CWP due to the inherently

greater riming potential. Each of the primary maxima in CWP is oriented along the terrain gradient region of windward slopes near where the strongest convergence-forced upslope occurs. It is of interest to note that the Park Range, including the location of SPL, exhibits a fair amount of cloud water during each of the four winters. There is very little high terrain to the west of the Park Range; thus, there is minimal moisture removal or subsidence drying that occurs to the west of SPL to limit orographic cloud formation. Furthermore, the north-south aligned ridge is ideal for maximized upslope conditions under predominant westerly wintertime flow. During less common southwesterly flow conditions, this region has inhibited cloud formation. The CWP plot for 2005 also clearly displays a general void of supercooled cloud water in the central region of Colorado extending from New Mexico to Wyoming. Even the Front Range and Eastern Plains exhibit some CWP resulting from easterly upslope flow. This central region void supports the hypothesis of Hindman (1986) in which orographic cloud formation and riming can be inhibited in mountainous terrain downwind of primary topographic barriers that act as an initial block to the predominant flow. Plots of the change in CWP due to increasing aerosols, not shown, reveal an increase in CWP along the mountain barriers where the spillover effect is most prominent. This increase results from reduced removal of supercooled liquid cloud water by riming.

The time averaged ice water path (IWP), shown in figure 11, displays a similar inter-seasonal trend to the total precipitation, with 2005 and 2008 exhibiting the greatest IWP state-wide. (The IWP includes the condensate from all ice hydrometeor species.) The fields of IWP do not exhibit a void in central Colorado. In the heavier snowfall seasons IWP is maximized along the primary mountain barriers as well as the central high mountain that include the major ski resorts of Summit County. In the central mountains, the high IWP and low CWP suggest ample snowfall for a given season that is not as strongly impacted by changes in aerosol concentration

as are upstream mountain ranges. The greatest local maxima in IWP coincide with the maxima in CWP due to strong upslope in these primary convergence zones. These co-located maxima are optimal for riming enhancement of snowfall as well as inhibition of riming by indirect aerosol effects. The Park Range of north-central Colorado also appears as an optimal location for orographically enhanced ice condensate regardless of the winter season. With a similar trend in CWP, this makes the Park Range consistently susceptible to aerosol impacts on seasonal snowfall. While the San Juan region provides the greatest continuous expanse of high levels of IWP, CWP, and snowfall spillover in 2005 and 2008, there is not a consistent inter-seasonal trend; moist, southwesterly flow is necessary for maximum orographic enhancement and aerosol impacts.

f. River Basin Hydrology

Identification of the potential precipitation spillover effect is critical with respect to the re-distribution of water resources among neighboring river basins in Colorado. The fields of total precipitation (fig 2) and total precipitation change (fig 7) were divided into river basins regions within Colorado as defined by the U.S. Geological Survey. Figure 12 displays the fields of (a) topography, (b) basin summed accumulated precipitation volume, (c) *change* in basin summed accumulated precipitation volume due to an increase in maximum aerosol concentration from CL to HP, and (d) *percentage change* represented by panel (c). For this analysis, it was chosen to present only the results from 2005 since this season experienced the greatest precipitation totals and spillover effect due to aerosol loading. In this figure, each river basin is numbered, and each number is identified in the river basin list in Table 2. The units of volume accumulated precipitation in figure 12 are acre-feet, which is used by water resource management to

document household water consumption and reservoir holdings throughout the state. After decomposing the precipitation change field from figure 2 into separate water basins, it is seen in panel c of figure 12 that upwind western basins generally experience a precipitation loss while downwind basins, clustered in central Colorado, receive a precipitation gain. The Upper San Juan (069) and Rio Grand Headwaters (049) basins experience the single greatest shift in total water volume between adjacent basins due to the aerosol influence. Upper San Juan basin loses more than 80,000 acre-feet while Rio Grand Headwaters gains more than 30,000 acre-feet. These spillover totals represent approximately a 3-5% loss of water in Upper San Juan and 2-3% gain in water in the Rio Grande Headwaters. The spillover across the Park Range from Upper Yampa (072) to the North Platte Headwaters (041) is also quite substantial. In the plot of percentage change in precipitated water volume, the values are high along the eastern border of the domain, which constitutes the lower elevation plains east of the Front Range Mountains. This area receives markedly less total seasonal precipitation than in the high terrain, so a small change in seasonal precipitation manifests as a large percentage difference but with only a small magnitude change in water volume.

g. Variability in Model Resolution

Given that spatial patterns and intensity of precipitation are strongly tied to the topography of Colorado it would be ideal to run model simulations at very high resolution to provide the best possible representation of the topography. However, in numerical modeling there is always a balance to be found between choosing the model grid spacing and the amount of wall clock time required to complete the given simulations. Following the suite of simulations at 3km grid spacing, several simulations were run at 1km grid spacing for the month of January

2005 over the San Juan Range. The new grid box encompassed the rectangular partition located in the southwest corner of the domain shown in figure 7a. This region and season were chosen because 2005 was the heaviest snowfall season of those simulated here and the San Juans experience a broad and high magnitude spillover effect. Simulations were run with the same aerosol profiles used in the 3km model runs. Figure 13 displays the modeled precipitation change for an increase in aerosols from CL to HP over the San Juan grid box area from both the 3km and 1km grid spacing simulations. The high resolution simulation produces much greater detail in the topography as well as the resulting precipitation change features. It also leads to a 4.2% increase in domain volume SWE. While there are changes in the details, the spillover effect is broadly similar between the two simulations both spatially and in magnitude, though the gain and loss maxima appear greater at the finer grid spacing. The spillover features tend to be smoother and horizontally continuous in the coarser simulations given that the topography is represented in that manner at the 3km scale. Table 3 provides precipitation information, similar to Table 1, to compare the San Juan region for the month of January 2005 at 3km and 1km grid spacing. In both the 3km and 1km spacing simulations there is a net loss in accumulated volume precipitation, though it does not exceed -1.50% even for an increase in aerosols from CL to HP. The majority of the aerosol impact, with respect to total volume increase and decrease, horizontal area impacted, and maximum grid point change, is achieved for an increase in aerosols from CL to MP. A further increase in aerosol concentration continues to impose similar trends in precipitation modification, but to a lesser degree.

4. Summary and Conclusions

The cloud-nucleating-aerosol indirect effect impacts wintertime precipitation in the high elevation mountain ranges of Colorado via the riming collection process as snow crystals advect or settle through moutaintop supercooled liquid water orographic clouds (Hindman et al. 1986; Rauber et al 1986; Borys et al. 2003; Saleeby et al. 2009). In several modeling studies, Saleeby and Cotton (2005) and Saleeby et al. (2006, 2007, 2009) examined the impact of increasing hygroscopic aerosol concentration on the resulting snowfall during winter weather events in 2004, 2005, and 2007, with emphasis on the north-central Park Range in Colorado. Results indicated that high aerosol concentrations tended to impede the riming process, resulting in unrimed or lightly rimed ice hydrometeors with a lower density and slower fall speeds. This translated into a precipitation spillover effect, whereby, precipitation amounts are reduced on windward slopes and enhanced on leeward slopes with only modest net precipitation suppression across the region. The work presented here consists of a follow-on modeling study intended to examine the aerosol-induced precipitation spillover effect across all of Colorado's mountainous regions on seasonal timescales.

The Colorado State University – Regional Atmospheric Modeling System (Walko et al. 1995; Meyers et al. 1997; Cotton et al. 2003; Saleeby and Cotton 2004, 2008) was used to simulate winter snowfall events from January 1 – March 1 of 2005, 2006, 2007, and 2008 within a nested grid framework at a grid spacing of 3km. Follow up simulations were performed for the month of January 2005 over the San Juan mountain range at 1km grid spacing. For each season, three simulations were performed with different vertically decreasing aerosol concentration profiles with maximum concentrations of 100, 800, and 1500 cm^{-3}, thus, respectively, representing clean (CL), moderately polluted (MP), and highly polluted (HP) environments.

From these multi-seasonal sensitivity simulations it was sought to examine: 1) the degree of inter-seasonal variability in aerosol effects on snowfall, 2) the spatial variability in cloud liquid water path, ice water path, accumulated snowfall, and the spillover effect, 3) the distribution of the spillover effect relative to the hydrological river basins in Colorado, and 4) the variability in numerically simulating this aerosol effect at 3km and 1km grid spacing.

The primary results of these simulations are as follows:

1. The magnitude of the aerosol spillover effect was greatest in the heaviest snowfall seasons of 2005 and 2008. This stems from greater orographically enhanced CWP and IWP during these seasons. Maxima in CWP were generally confined to mountain ridge locations while IWP was widespread across the mountainous regions of CO. As such, the spillover effect was maximized where CWP and IWP co-existed and were local maxima.
2. Of the major CO mountain ranges, the San Juan Range is the overall highest and largest in expanse, and it typically boasts the greatest snowfall accumulations in the state. In the simulations it exhibited the greatest spatially continuous snowfall spillover effect compared to the other major mountain ranges.
3. The central high mountains of Colorado experienced a relatively small spillover effect compared to the primary upstream mountain barriers. This results from a relative absence of supercooled liquid water clouds and very little or infrequent riming growth of snow crystals in these central mountain ranges. Less orographic cloud water is likely attributed to upstream moisture removal or subsidence drying in the wake of the western slope mountain barriers.
4. During heavy snowfall winters, the seasonal spillover effect is a composite of many individual episodes rather than the result of a single large event. Mountain ranges prone

to orographic liquid water cloud development tend to have frequent episodes during winters that are favorable for their development.

5. Of the simulated seasons, the maximum net change in domain total precipitated water volume, on the Colorado 3km grid spacing domain, resulting from an increase in aerosols from CL to HP, was a reduction of only -1.48%. The maximum spillover loss was -2.96% and gain was 1.48%.
6. In a comparison of the San Juan region on the 3km and 1km grid spacing domains, the 1km spacing domain produced finer scale spillover features, a slightly greater net snowfall loss (-1.47% compared to -1.17%), greater spillover volume loss (-4.06% to -3.12%), greater spillover volume gain (2.59% to 1.95%), and greater maximum grid point loss (-158.66mm to -93.06mm) and gain (72.96mm to 40.90mm). While the maximum magnitudes changed substantially on the finer grid, both grids produced similar spatial variability in the spillover effect relative to the highest terrain.

From this numerical investigation, it has become apparent that the impact of cloud nucleating aerosols is largely controlled by the synoptic scale flow and available moisture. While the inter-seasonal synoptic variability exerts a larger control than aerosols over snowfall variability, studying aerosol impacts is important for our understanding of how snowfall magnitudes and spatial distributions can be modulated by pollution levels within a given winter season. While some localized mountainous regions would be susceptible to aerosol effects during any given winter, the potential broad scale effects seen in the simulations of the 2005 and 2008 seasons require above normal moisture and strong northwesterly or southwesterly flow. The direction of this flow further determines the locations that are most primed for orographic cloud formation

and potential riming growth of ice hydrometeors. Under ideal flow conditions for a substantial snowfall winter, and with an above normal level of nucleating aerosols, the potential is high for a downwind redistribution of the winter snowpack.

Acknowledgements: This work was supported by the National Science Foundation Division of Atmospheric Sciences grant ATM-0835421.

5. References

Albrecht, B., 1989: Aerosols, cloud microphysics, and fractional cloudiness. Science, **245**, 1227-1230.

Borys, R.D., and M.A. Wetzel, 1997: Storm Peak Laboratory: A research, teaching and service facility for the atmospheric sciences. *Bull. Amer. Meteor. Soc.*, **78**, 2115-2123.

_____, D. H. Lowenthal, and D. L. Mitchell, 2000: The relationships among cloud microphysics, chemistry, and precipitation rate in cold mountain clouds. *Atmos. Environ*., **34**, 2593–2602.

_____, _____, S. A. Cohn, and W. O. J. Brown, 2003: Mountaintop and radar measurements of anthropogenic aerosol effects on snow growth and snowfall rate. *Geophys. Res. Lett*., **30**, 1538, doi:10.1029/2002GL016855.

Cober, S.G. and R. List, 1993: Measurements of the heat and mass transfer parameters characterizing conical graupel growth. *J. Atmos. Sci.*, **50**, 1591-1609.

Colle, B.A., 2004: Sensitivity of orographic precipitation to changing ambient conditions and terrain geometries: An idealized modeling perspective. *J. Atmos. Sci*., **61**, 588-606.

_____, J.B. Wolfe, W.J. Steenburgh, D.E. Kingsmill, J.A.W. Cox, J.C. Shafer, 2005: High-resolution simulations and microphysical validation of an orographic precipitation event over the Wasatch Mountain during IPEX IOP3. *Mon. Wea. Rev*., **133**, 2947-2971.

_____, 2008: Two-dimensional idealized simulations of the impact of multiple windward ridges on orogrpahic precipitation. *J. Atmos. Sci*., **65**, 509-523.

Cotton, W.R., R.A. Pielke, Sr., R.L. Walko, G.E. Liston, C.J. Tremback, H. Jiang, R.L. McAnelly, J.Y. Harrington, M.E. Nicholls, G.G. Carrió, J.P. McFadden, 2003: RAMS 2001: Current status and future directions. *Meteor. Atmos Physics*, **82**, 5-29.

Fraser, A., R. Easter, and P. Hobbs, 1973: A theoretical study of the flow of air and fallout of solid precipitation over mountainous terrain: Part I. Airflow Model. *J. Atmos. Sci.*, **30**, 813-823.

Givati, A., and D. Rosenfeld, 2004: Quantifying precipitation suppression due to air pollution. *J. Appl. Meteor*., **43,** 1038–1056.

Greenan B.J.W. and R. List, 1995: Experimental closure of the heat and mass transfer theory of spheroidal hailstones. *J. Atmos. Sci.*, **52**, 3797-3815.

Harrington, J.Y., 1997: The effects of radiative and microphysical processes on simulated warm and transition season Arctic stratus. PhD Diss., Atmospheric Science paper No. 637, Colorado State University, Dept of Atmos Sci, Fort Collins, CO, 289pp.

Heymsfield, A. J., and R. M. Sabin, 1989: Cirrus crystal nucleation by homogeneous freezing of solution droplets. *J. Atmos. Sci*., **46**, 2252-2264.

Hindman, E. E., 1986: Characteristics of supercooled liquid water in clouds at mountaintops in the Colorado Rockies. *J. Climate Appl. Meteor*., **25**, 1271–1279.

_____, E. Carter, R. Borys, and D. Mitchell, 1992: Collecting supercooled cloud droplets as a function of droplet size. *J. Atmos. Oceanic Tech*., **9**, 337-353.

Hobbs, P., R. Easter, and A. Fraser, 1973: A theoretical study of the flow of air and fallout of solid precipitation over mountainous terrain: Part II. Microphysics. *J. Atmos. Sci*., **30**, 813-823.

Jirak, I. L., and W. R. Cotton, 2006: Effect of air pollution on precipitation along the Front Range of the Rocky Mountains. *J. Appl. Meteorol. Climatol.*, **45**, 236–245.

Kain, J.S., and J.M. Fritsch, 1993: Convective parameterization for mesoscale models: The Kain-Fritsch scheme. *The Representation of Cumulus Convection in Numerical Models, Meteor. Monogr.*, No. 46, Amer. Meteor. Soc., 165-170.

Khain, A., and A. Pokrovsky, 2004: Effects of atmospheric aerosols on deep convective clouds as seen from simulations using a spectral microphysics mixed-phase cumulus cloud model, part 2: Sensitivity study, *J. Atmos. Sci*., **61**, 2983– 3001.

Khain, A., D. Rosenfeld, and A. Pokrovsky, 2005: Aerosol impact on the dynamics and microphysics of convective clouds, *Q. J. R. Meteorol. Soc*., **131**, 2639–2663.

Klemp, J.B., and R.B. Wilhelmson, 1978: The simulation of three-dimensional convective storm dynamics. *J. Atmos. Sci*., **35**, 1070-1096.

Korolev, A., 2007: Limitations of the Wegener–Bergeron–Findeisen mechanism in the evolution of mixed-phase clouds. *J. Atmos. Sci*., **64**, 3372-3375.

Lohmann, U., 2004: Can anthropogenic aerosols decrease the snowfall rate? *J. Atmos. Sci*., **61**, 2457-2468.

Lynn, B., A. Khain, D. Rosenfeld, and W. L. Woodley, 2007: Effects of aerosols on precipitation from orographic clouds, *J. Geophys. Res.*, **112**, D10225, doi:10.1029/2006JD007537.

Mellor, G.L., T. Yamada, 1974: A hierarchy of turbulence closure models for planetary boundary layers. *J. Atmos. Sci*., **31**, 1791-1806.

Mesinger, F., G. DiMego, E. Kalnay, K. Mitchell, P.C. Shafran, W. Ebisuzaki, D. Jović, J. Woollen, E. Rogers, E.H. Berbery, M.B. Ek, Y. Fan, R. Grumbine, W. Higgins, H. Li, Y. Lin, G. Manikin, D. Parrish, W. Shi, 2006: North American Regional Reanalysis. *BAMS*, 87, 343-360.

Meyers, M.P., R.L. Walko, J.Y. Harrington, and W.R. Cotton, 1997: New RAMS cloud microphysics parameterization. Part II. The two-moment scheme. *Atmos. Res*. **45**, 3-39.

Mitchell, D. L., R. Zhang, and R. L. Pitter, 1990: Mass dimensional relationships for ice particles and the influence of riming on snowfall rates. *J. Appl. Meteor*., **29**, 153–163.

Mossop, S.C., 1976: Production of secondary ice particles during the growth of graupel by riming. *Quart. J. Roy. Meteorol. Soc.*, **102**, 45-57.

Muhlbauer, A., and U. Lohmann, 2008: Sensitivity studies of the role of aerosols in warm-phase orographic precipitation in different dynamical flow regimes. *J. Atmos. Sci*., **65**, 2522-2542.

Muhlbauer, A., and U. Lohmann, 2009: Sensitivity studies of aerosol-cloud interactions in mixed-phase orographic precipitation. *J. Atmos. Sci*., **66**, 2517-2538.

Pitter, R. L., and H. R. Pruppacher, 1974: A numerical investigation of collision efficiencies of simple ice plates colliding with supercooled water drops. *J. Atmos. Sci*., **31**, 551–559.

Rauber, R.M., and L.O. Grant, 1986: The characteristics and distribution of cloud water over the mountains of northern Colorado during wintertime storms. Part II: Spatial distribution and microphysical characteristics. *J. Climate Appl. Meteor*., **25**, 489-504.

Reinking, R. F., J. B. Snider, and J. L. Coen, 2000: Influences of storm-embedded orographic gravity waves on cloud liquid water and precipitation. *J. Appl. Meteor*., **39**, 733–759.

Rosenfeld, D., and A. Givati, 2006: Evidence of orographic precipitation suppression by air pollution–induced aerosols in the western United States. *J. Appl. Meteorol.Climatol.,* **45**, 893-911.

Rutunno, R., and R.A. Houze, 2007: Lessons on orographic precipitation from the Mesoscale Alpine Programme. *Quart. J. Roy. Meteor. Soc*., **133**, 811-830.

Saleeby, S.M., R.D. Borys, M.A. Wetzel, D. Simeral, M.P. Meyers, W.R. Cotton, R. McAnelly, N. Larson, E. Heffernan, 2006: Model aerosol sensitivity studies and microphysical interactions in an orographic snowfall event. *12th Conference on Mountain Meteorology*, Santa Fe, NM.

_____, and W.R. Cotton, 2004: A large droplet mode and prognostic number concentration of cloud droplets in the Colorado State University Regional Atmospheric Modeling System (RAMS). Part I: Module descriptions and supercell test simulations. *J. Appl. Meteor.*, **43**, 182-195.

_____, _____, 2005: A large-droplet mode and prognostic number concentration of cloud droplets in the Colorado State University Regional Atmospheric Modeling System (RAMS). Part II: Sensitivity to a Colorado winter snowfall event. *J. Appl. Meteor.*, **44**, 1912-1929.

_____, _____, R.D. Borys, D. Lowenthal, and M.A. Wetzel, 2007: Relative impacts of orographic forcing and pollution aersosols on mountain snowfall. *12th Conference on Mesoscale Processes*, Waterville Valley, NH.

_____, _____, 2008: A binned approach to cloud-droplet riming implemented in a bulk microphysics model**.** *J. Appl. Meteorol.Climatol.,* **47**, 694-703.

_____, _____, D. Lowenthal, R.D. Borys, and M.A. Wetzel, 2009: Influence of cloud condensation nuclei on orographic snowfall. *J. Appl. Meteor. & Clim.,* **48**, 903-922.

Smagorinsky, J., 1963: General circulation experiments with the primitive equations. *Mon. Wea. Rev.*, **91**, 99-164.

Smith, R.B., I. Barstad, and L. Bonneau, 2005: Orographic precipitation and Oregon's climate transition. *J. Atmos. Sci*., **62**, 177-191.

Tzivion, S., G. Feingold, and Z. Levin, 1987: An efficient numerical solution to the stochastic collection equation. *J. Atmos. Sci.*, **44**, 3139-3149.

Walko, R. L., W. R. Cotton, M. P. Meyers, and J. Y. Harrington, 1995: New RAMS cloud microphysics parameterization: Part I. The single-moment scheme. *Atmos. Res*., **38**, 29–62.

Walko, R.L., and Coauthors, 2000: Coupled atmosphere-biophysics-hydrology models for environmental modeling. *J. Appl. Meteor*., **39**, 931-944.

Wang, P. K., and W. Ji, 2000: Collision efficiencies of ice crystals at low-intermediate Reynolds numbers colliding with supercooled cloud droplets: A numerical study. J. *Atmos. Sci*., **57**, 1001–1009.

Wetzel, M.A., M. Meyers, R. Borys, R. McAnelly, W.R. Cotton, A. Rossi, P. Frisbie, D. Nadler, D. Lowenthal, S. Cohn, W. Brown, 2004: Mesoscale snowfall prediction and verification in mountainous terrian. *Wea. Forecasting*, **19**, 806-828.

6. Tables

Table 1. Positive and negative precipitation changes due to the increase in aerosol concentration is given in Column 1. All four simulated seasons are shown. Columns 2-4 give the net, decrease (Dec), and increase (Inc) percentage change in domain summed SWE volume. Columns 5-6 display the percentage of domain area that experiences a decrease and increase in SWE of at least 5mm. Columns 7-8 present the domain grid point maximum decrease and increase in SWE.

Table 2. List of the river basins that are labeled and numbered in the plots of changes in river basin accumulated precipitation.

Table 3. Same as Table 1, except that precipitation information is given from the 3km and 1km grid spacing simulations that cover the San Juan region for the month of January 2005.

7. Figures

Figure 1. The top panel displays the 3-grid configuration. The outer Grid-1 uses 36km grid spacing and encompasses the full figure panel. Grid-2 is displayed in the light blue color and has a grid spacing of 12km. Grid-3 is shown by the darker blue color and has a grid spacing of 3km. The bottom panel displays the topography (meters) on grid-3. Outlined and numbered boxes indicate the: 1) Park Range, 2) Summit County Region, 3) Flat Tops, 4) San Juan Range, 5) Grand Mesa, and 6) Uncompahgre Plateau. The location of Storm Peak Lab (SPL) is indicated in Region 1.

Figure 2. Total accumulated (60-day) precipitation (mm) on the 3km grid spacing domain over Colorado for the clean simulations. Precipitation is color shaded and topography (m) is contoured and labeled. The following SNOTEL sites are indicated: Rabbit Ears Pass (RAB), Joe Wright Reservoir (JOE), Overland Reservoir (OVR),Wolf Creek Summit (WLF), Columbine Pass (COL), and Sharkstooth (SKZ).

Figure 3. Composite 500mb geopotential height (m) from the NARR dataset for 1 Jan – 1 Mar: (a) 2005, (b) 2006, (c) 2007, and (d) 2008.

Figure 4. Composite 500mb geopotential height anomaly (m) from the NARR dataset for 1 Jan – 1 Mar: (a) 2005, (b) 2006, (c) 2007, and (d) 2008. Long term means for anomaly computation run from 1979-2007.

Figure 5. Composite 700mb relative humidity anomaly (%) from the NARR dataset for 1 Jan – 1 Mar: (a) 2005, (b) 2006, (c) 2007, and (d) 2008. Long term means for anomaly computation run from 1979-2007.

Figure 6. Time series of SNOTEL SWE (mm, solid lines) for 60 days beginning 1 Jan for the 2005-2008 winter seasons. The SNOTEL site names indicated on figure 2 are labeled on each panel. Corresponding model time series from grid points closest to SNOTEL sites are given (dashed lines) as well as the time series from 2 grid points down-slope (dotted lines) of the SNOTEL location. Lines are color coded by year as labeled on the plot.

Figure 7. Difference in total accumulated (60-day) precipitation (mm) on the 3km grid spacing domain over Colorado between the highly polluted and clean simulations. Precipitation is color shaded and topography (m) is contoured and labeled. Negative (positive) values indicate a decrease (increase) in precipitation for an increase in aerosol concentration. Rectangular partition in (a) represents the zoomed region shown in figure 13.

Figure 8. Time series from several grid points of (a) accumulated SWE (mm) from the 2005 seasonal simulation with maximum aerosol concentration of 100 cm^{-3}, and (b) change in accumulated SWE (mm) resulting from an increase in maximum aerosol concentration from 100 to 1500 cm^{-3}. The time series indicated by "Max Loss Point" is taken from the domain grid point with the maximum loss in SWE due to aerosol loading (located in the San Juan Range at 37.81N, -106.81W). The time series for "Relative Gain Point" was taken from the grid point downwind of "Max Loss Point" that represents the maximum local gain in SWE (37.35, -106.56), and "Near Neutral Point" is located along the ridge between the other two locations where the total change in SWE is near zero (37.32, -106.67).

Figure 9. Cloud droplet number concentration (CDNC, cm^{-3}, markers) averaged over all cloudy grid cells every three hours for the duration of the 60-day simulations initialized with clean (red diamonds), polluted (blue squares), and highly polluted (black triangles) aerosol profiles. Also shown is the percent of domain grid cells containing cloud water of at least 0.05 g kg^{-1} (black contours) for the clean simulations. The panels are from the snow seasons of (a) 2005, (b) 2006, (c) 2007, and (d) 2008. CDNC is only averaged over grid cells with a cloud water content minimum of 0.05 g kg^{-1}.

Figure 10. Mean cloud liquid water path (CWP) (mm x 1000) time averaged at 3-hourly intervals over 60 days on the 3km grid spacing domain. CWP is color shaded and topography (m) is contoured and labeled.

Figure 11. Mean ice water path (IWP) (mm x 1000) time averaged at 3-hourly intervals over 60 days on the 3km grid spacing domain. IWP is color shaded and topography (m) is contoured and labeled.

Figure 12. Simulated model variables divided into Colorado River Basins (outline in bold, black lines): (a) topography (m), (b) total accumulated basin volume precipitation (acre-feet / 1000) from the simulation with maximum aerosol concentration of 100 cm^{-3}, (c) change in basin volume precipitation (acre-feet / 1000) for an increase in maximum aerosol concentration from 100 to 1500 cm^{-3}, (d) same as (c) but given as % change. Basins are numbered according to Table 2.

Figure 13. Difference in January 2005 accumulated (30-day) precipitation (mm) on the (a) 3-km and (b) 1-km grid spacing domains over Colorado between the highly polluted and clean simulations. Precipitation is color shaded and topography (m) is contoured and labeled. Negative (positive) values indicate a decrease (increase) in precipitation for an increase in aerosol concentration. The domain shown here covers the San Juan Range and is indicated by the rectangle partition in figure 7a.

Table 1. Positive and negative precipitation changes due to the increase in aerosol concentration is given in Column 1. All four simulated seasons are shown. Columns 2-4 give the net, decrease (Dec), and increase (Inc) percentage change in domain summed SWE volume. Columns 5-6 display the percentage of domain area that experiences a decrease and increase in SWE of at least 5mm. Columns 7-8 present the domain grid point maximum decrease and increase in SWE.

Maximum Aerosol Change	Total SWE Net %change Volume	Total SWE Dec %change Volume	Total SWE Inc %change Volume	Threshold SWE Dec %change Area	Threshold SWE Inc %change Area	Max Point SWE Dec (mm)	Max Point SWE Inc (mm)
Year 2005							
100 to 800	-0.74	-2.14	1.40	-31.93	21.49	-119.10	60.03
800 to 1500	-0.76	-1.34	0.58	-22.76	9.86	-52.26	27.17
100 to 1500	-1.48	-2.96	1.48	-39.84	20.26	-162.75	69.16
Year 2006							
100 to 800	-0.22	-0.90	0.68	-2.96	1.35	-25.93	13.83
800 to 1500	-0.03	-0.50	0.47	-0.21	0.21	-8.36	10.81
100 to 1500	-0.26	-1.09	0.83	-3.94	2.26	-34.29	19.63
Year 2007							
100 to 800	-0.35	-1.15	0.80	-8.12	5.45	-26.01	22.24
800 to 1500	0.10	-0.62	0.72	-2.65	2.53	-12.16	12.53
100 to 1500	-0.25	-1.37	1.12	-11.83	8.88	-34.34	24.77
Year 2008							
100 to 800	-0.40	-1.30	0.90	-13.15	9.99	-107.69	49.46
800 to 1500	-0.16	-0.59	0.43	-4.95	4.67	-33.11	13.65
100 to 1500	-0.56	-1.67	1.11	-15.55	13.11	-136.75	58.91

Table 2. List of the river basins that are labeled and numbered in the plots of changes in river basin accumulated precipitation.			
1	Alamosa Trinchera	38	Middle South Platte / Sterling
2	Animas	39	Montezuma
3	Apishapa	40	Muddy
4	Arkansas Headwaters	41	North Platte Headwaters
5	Big Sandy	42	North Fork Gunnison
6	Big Thompson	43	Parachute Roan
7	Bijou	44	Pawnee
8	Bitter	45	Piceance Yellow
9	Blue	46	Piedra
10	Cache La Poudre	47	Purgatorie
11	Canadian Headwaters	48	Rio Chama
12	Chico	49	Rio Grand Headwaters
13	Cimarron	50	Roaring Fork
14	Clear	51	Rush
15	Colorado Headwaters	52	Saguache
16	Colorado Headwaters Plateau	53	San Luis
17	Conejos	54	San Miguel
18	Crow	55	Sidney Draw
19	Eagle	56	South Platte Headwater
20	East Taylor	57	St. Vrain
21	Fountain	58	Tomichi
22	Horse	59	Uncompahange
23	Huerfano	60	Upper Arkansas
24	Kiowa	61	Upper Arkansas / Lake Meredith
25	Little Snake	62	Upper Dolores
26	Lone Tree Owl	63	Upper Green / Flaming Gorge Res
27	Lower Dolores	64	Upper Gunnison
28	Lower Green Diamond	65	Upper Laramie
29	Lower Gunnison	66	Upper Lodgepole
30	Lower Lodgepole	67	Upper North Platte
31	Lower San Juan / Four Corners	68	Upper Rio Grande
32	Lower White	69	Upper San Juan
33	Lower Yampa	70	Upper South Platte
34	Mancos	71	Upper White
35	Mcelmo	72	Upper Yampa
36	Middle San Juan	73	Vermilion
37	Middle South Platte / Cherry Creek	74	Westwater Canyon

Table 3. Same as Table 1, except that precipitation information is given from the 3km and 1km grid spacing simulations that cover the San Juan region for the month of January 2005.

Maximum Aerosol Change	Total SWE Net %change Volume	Total SWE Dec %change Volume	Total SWE Inc %change Volume	Threshold SWE Dec %change Area	Threshold SWE Inc %change Area	Max Point SWE Dec (mm)	Max Point SWE Inc (mm)
3km Grid							
100 to 800	-0.91	-2.26	1.35	-21.60	14.77	-72.14	32.28
800 to 1500	-0.27	-1.02	0.75	-12.13	9.12	-25.12	13.88
100 to 1500	-1.17	-3.12	1.95	-26.38	23.39	-93.06	40.90
1km Grid							
100 to 800	-0.88	-2.95	2.07	-31.98	23.52	-123.74	52.39
800 to 1500	-0.61	-1.40	0.79	-18.08	11.93	-37.70	22.65
100 to 1500	-1.47	-4.06	2.59	-37.61	25.33	-158.66	72.96

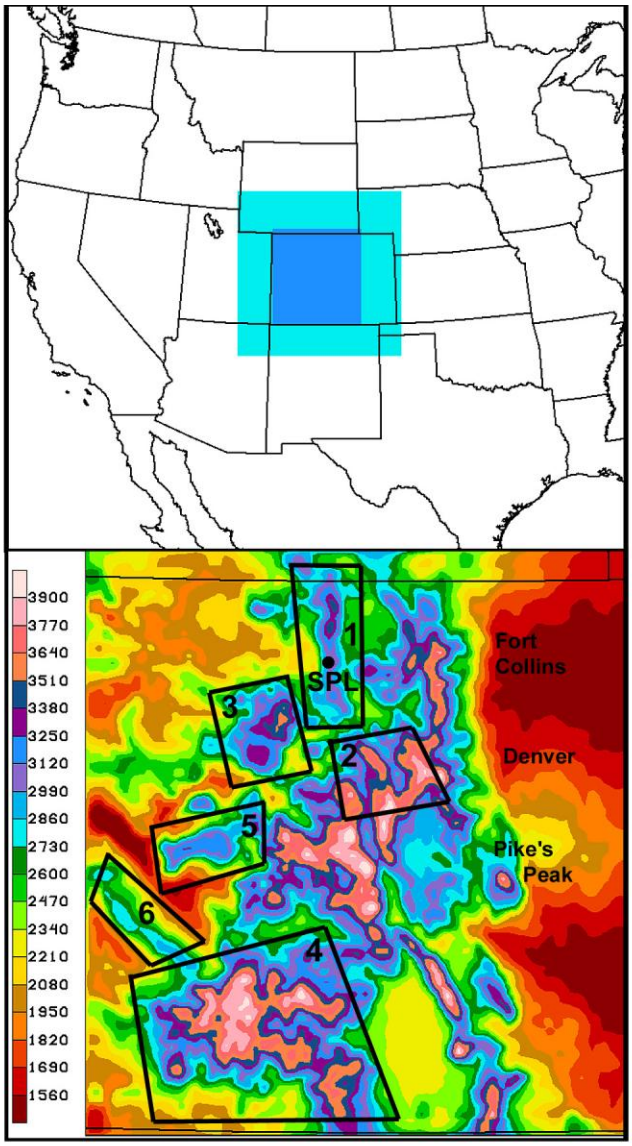

Figure 1. The top panel displays the 3-grid configuration. The outer Grid-1 uses 36km grid spacing and encompasses the full figure panel. Grid-2 is displayed in the light blue color and has a grid spacing of 12km. Grid-3 is shown by the darker blue color and has a grid spacing of 3km. The bottom panel displays the topography (meters) on grid-3. Outlined and numbered boxes indicate the: 1) Park Range, 2) Summit County Region, 3) Flat Tops, 4) San Juan Range, 5) Grand Mesa, and 6) Uncompahgre Plateau. The location of Storm Peak Lab (SPL) is indicated in Region 1.

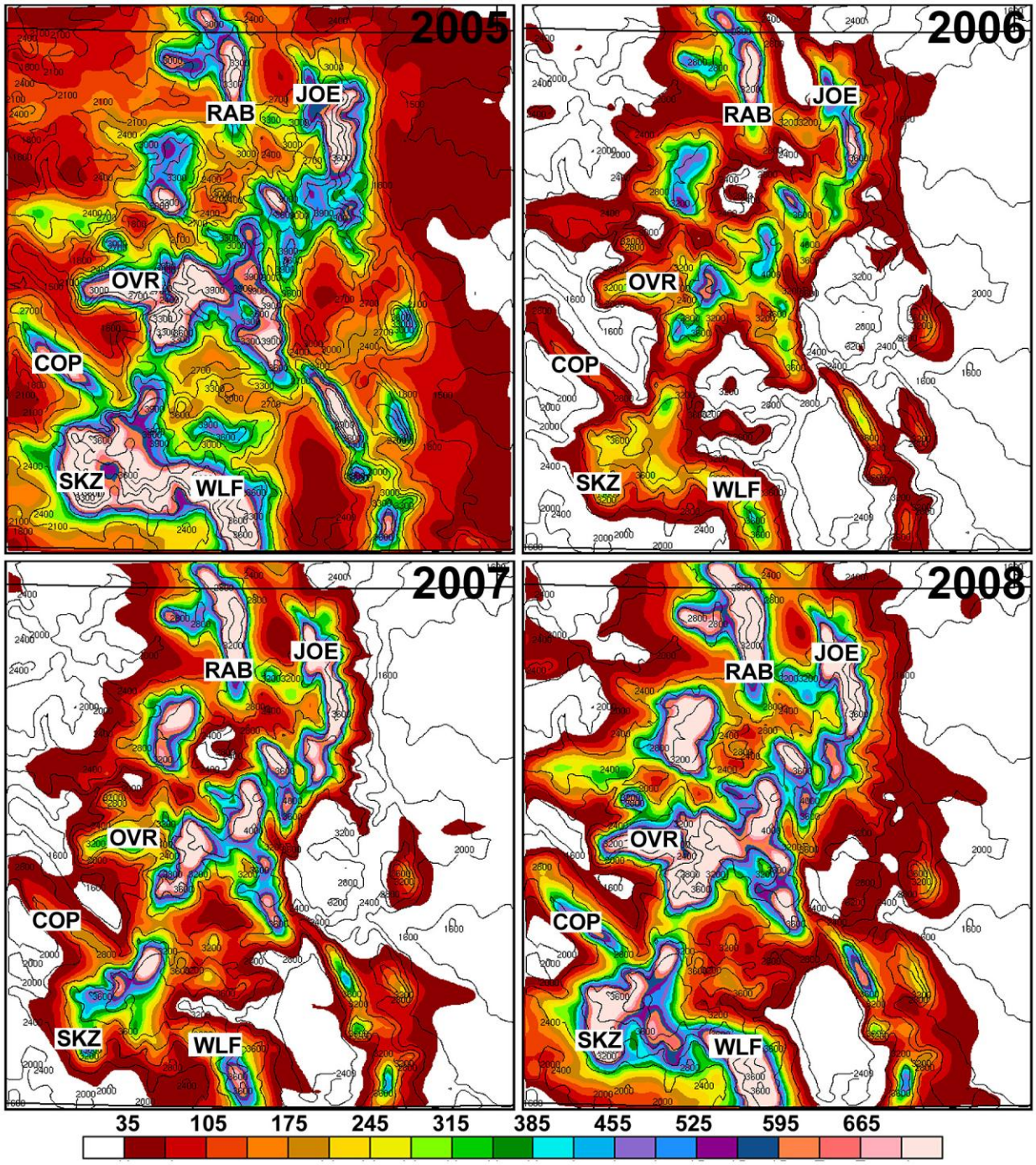

Figure 2. Total accumulated (60-day) precipitation (mm) on the 3km grid spacing domain over Colorado for the clean simulations. Precipitation is color shaded and topography (m) is contoured and labeled. The following SNOTEL sites are indicated: Rabbit Ears Pass (RAB), Joe Wright Reservoir (JOE), Overland Reservoir (OVR),Wolf Creek Summit (WLF), Columbine Pass (COL), and Sharkstooth (SKZ).

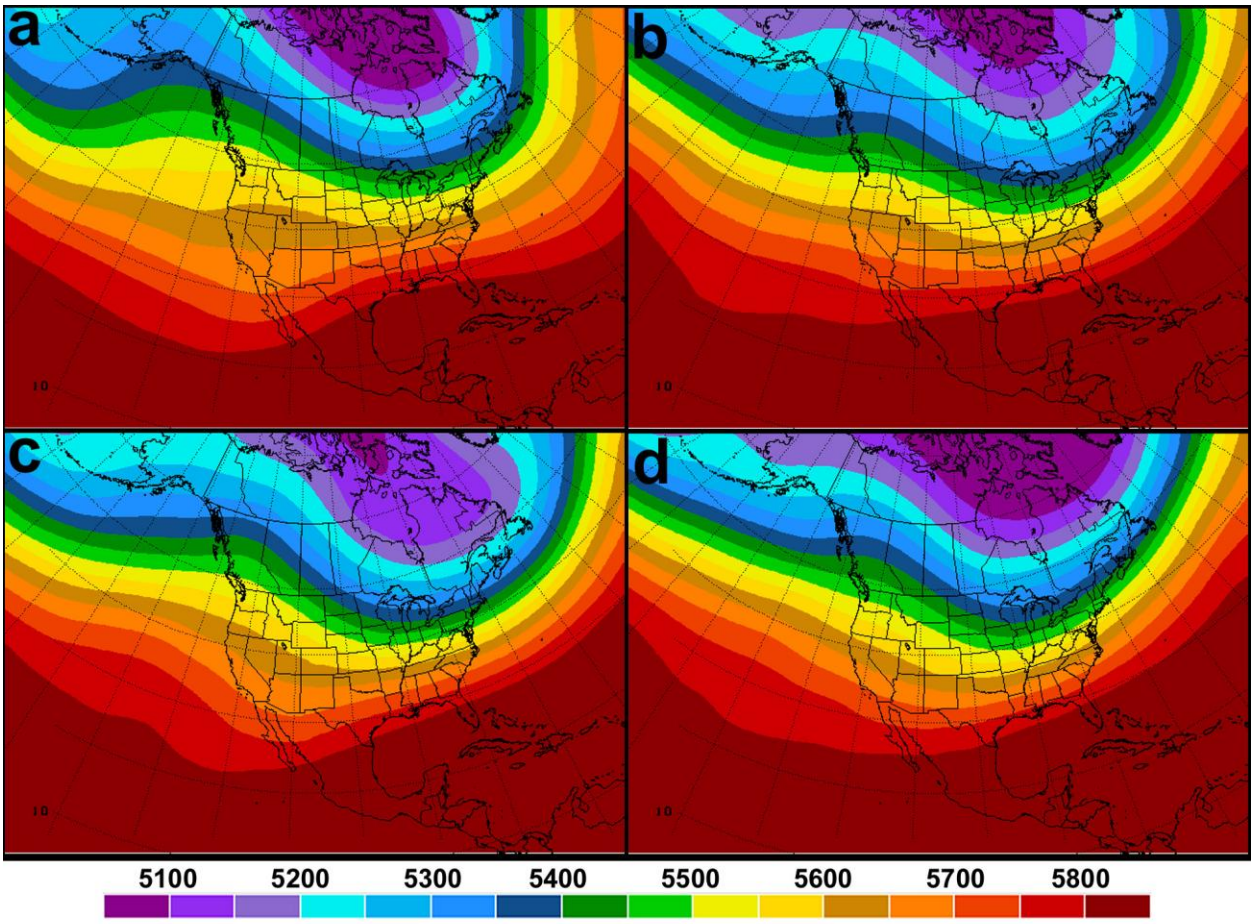

Figure 3. Composite 500mb geopotential height (m) from the NARR dataset for 1 Jan – 1 Mar: (a) 2005, (b) 2006, (c) 2007, and (d) 2008.

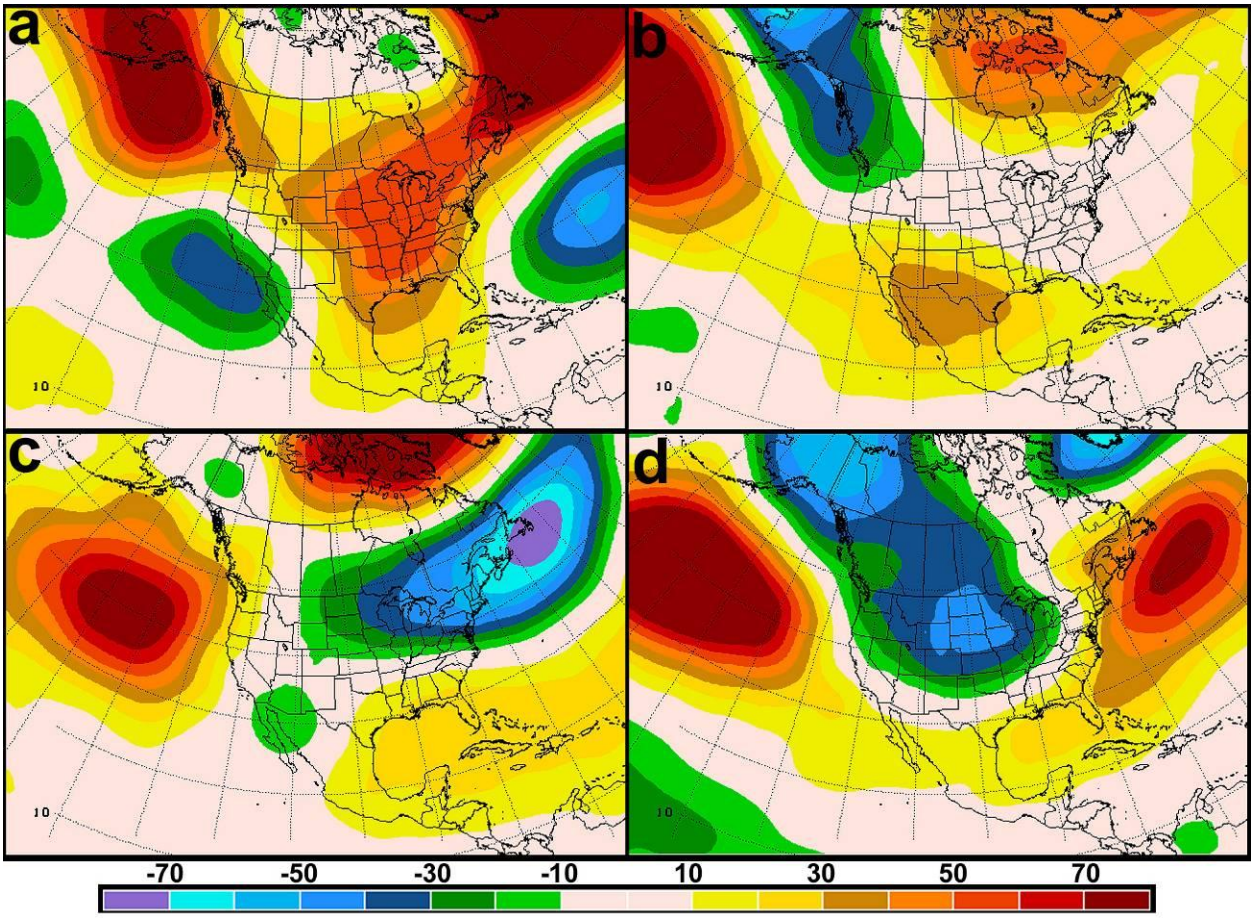

Figure 4. Composite 500mb geopotential height anomaly (m) from the NARR dataset for 1 Jan – 1 Mar: (a) 2005, (b) 2006, (c) 2007, and (d) 2008. Long term means for anomaly computation run from 1979-2007.

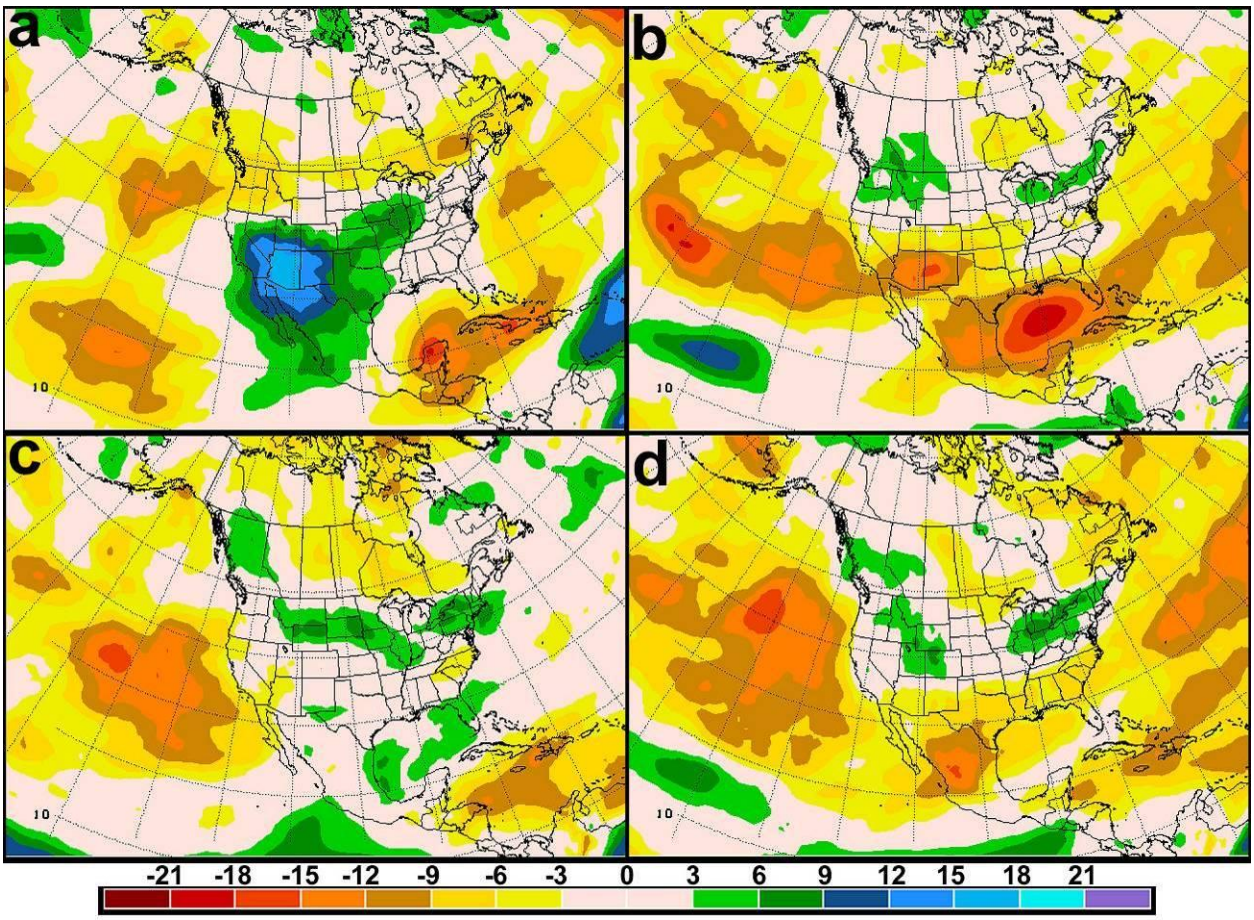

Figure 5. Composite 700mb relative humidity anomaly (%) from the NARR dataset for 1 Jan – 1 Mar: (a) 2005, (b) 2006, (c) 2007, and (d) 2008. Long term means for anomaly computation run from 1979-2007.

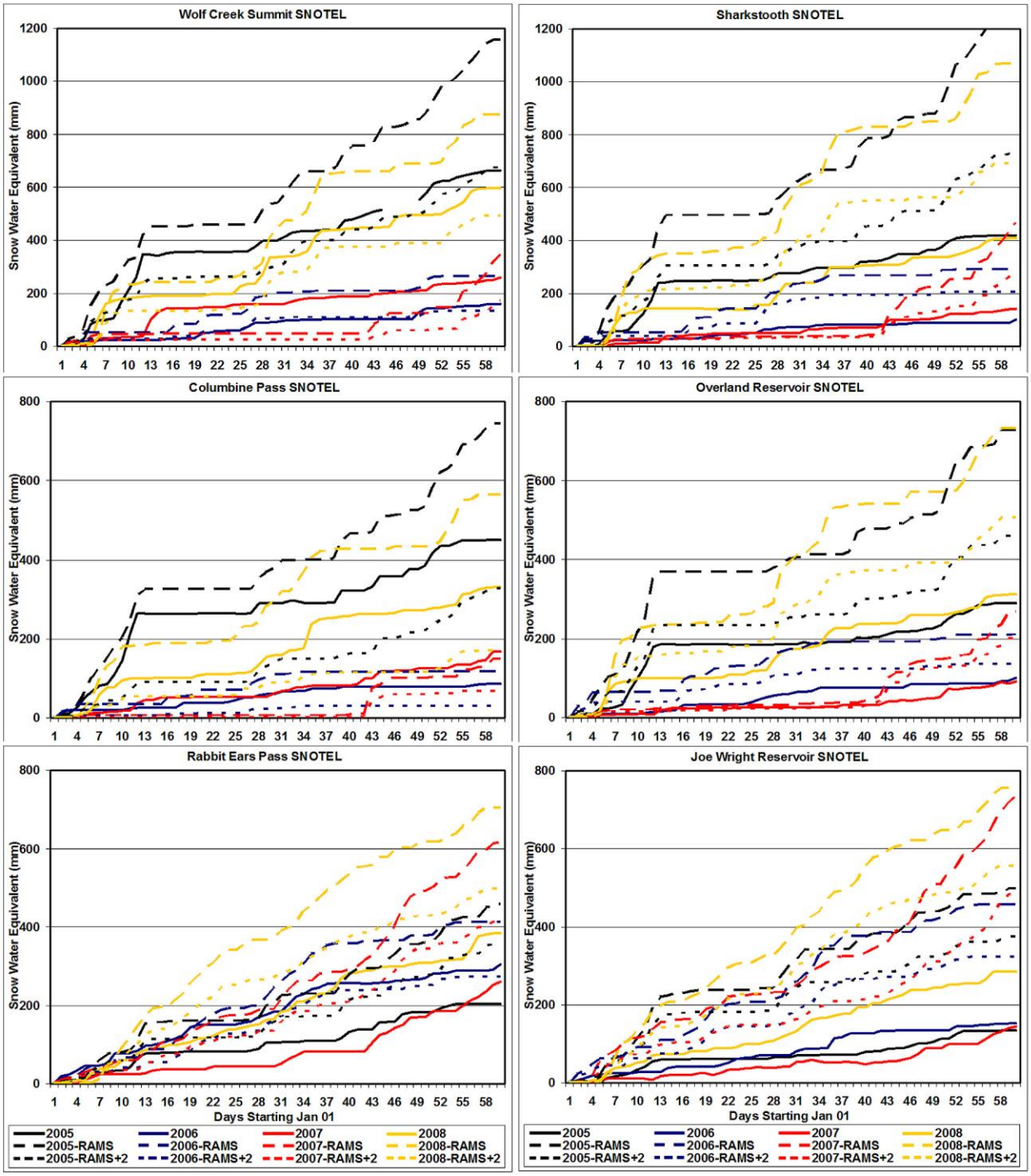

Figure 6. Time series of SNOTEL SWE (mm, solid lines) for 60 days beginning 1 Jan for the 2005-2008 winter seasons. The SNOTEL site names indicated on figure 2 are labeled on each panel. Corresponding model time series from grid points closest to SNOTEL sites are given (dashed lines) as well as the time series from 2 grid points down-slope (dotted lines) of the SNOTEL location. Lines are color coded by year as labeled on the plot.

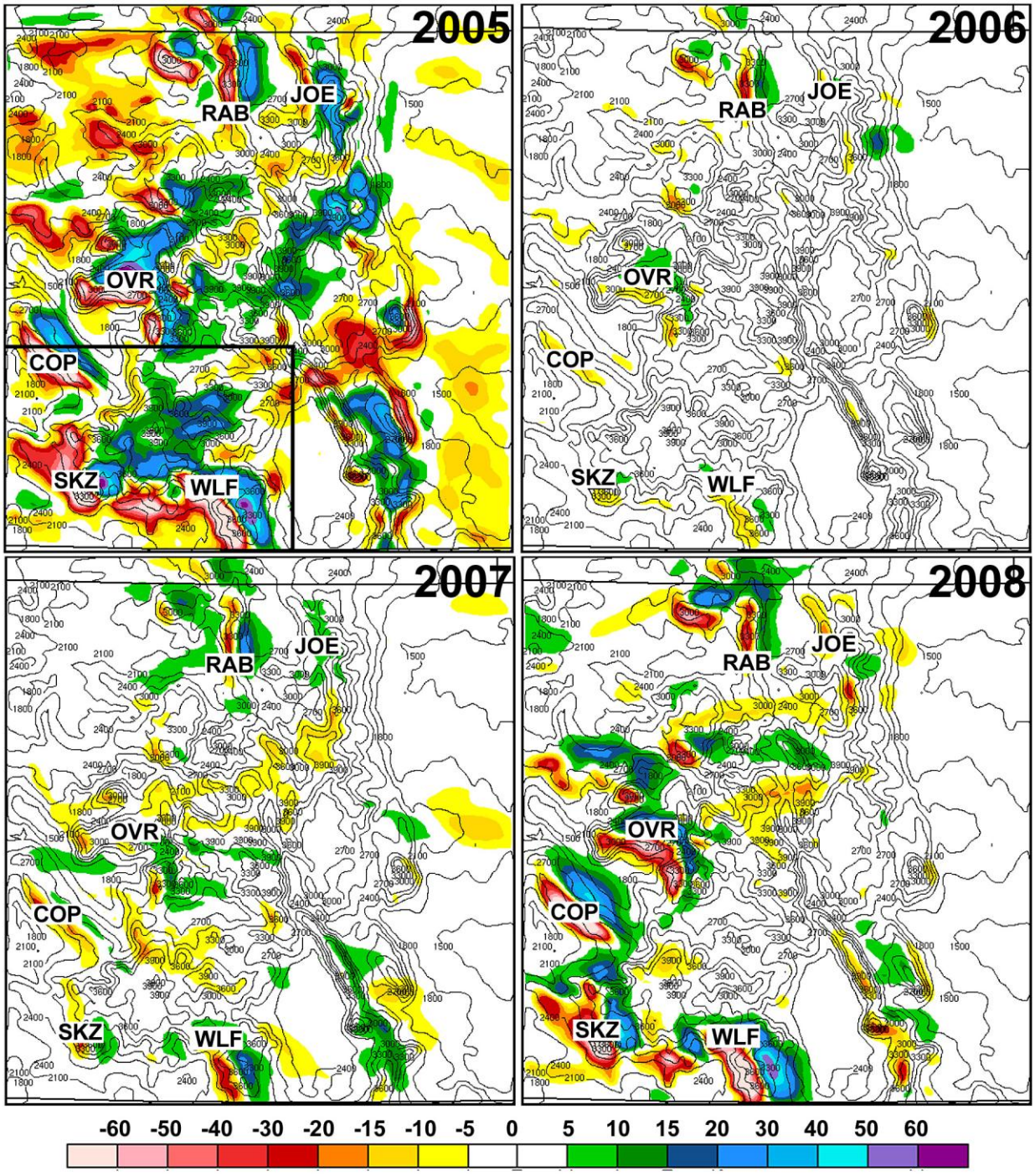

Figure 7. Difference in total accumulated (60-day) precipitation (mm) on the 3km grid spacing domain over Colorado between the highly polluted and clean simulations. Precipitation is color shaded and topography (m) is contoured and labeled. Negative (positive) values indicate a decrease (increase) in precipitation for an increase in aerosol concentration. Rectangular partition in (a) represents the zoomed region shown in figure 13.

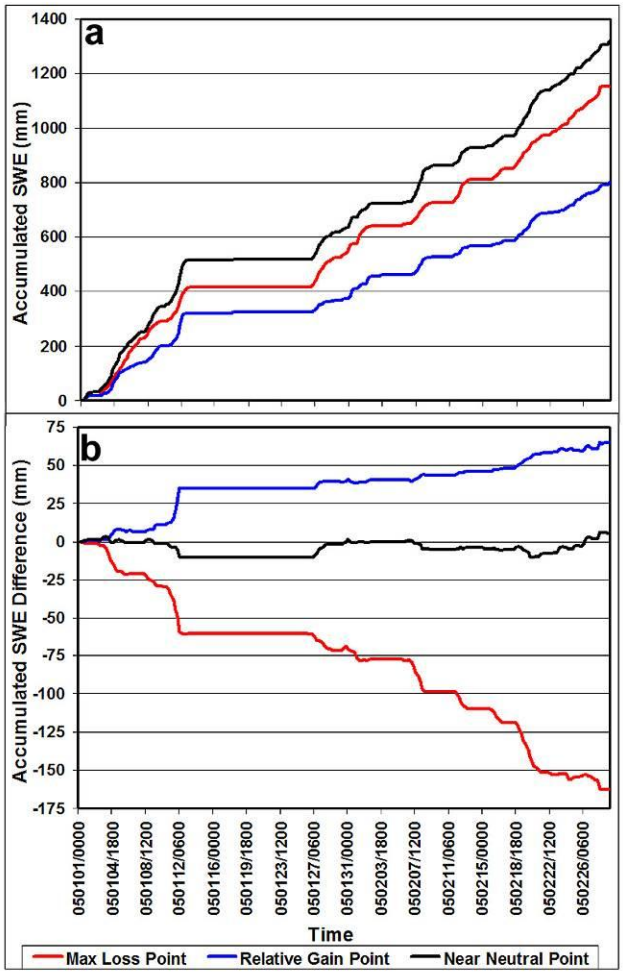

Figure 8. Time series from several grid points of (a) accumulated SWE (mm) from the 2005 seasonal simulation with maximum aerosol concentration of 100 cm^{-3}, and (b) change in accumulated SWE (mm) resulting from an increase in maximum aerosol concentration from 100 to 1500 cm^{-3}. The time series indicated by "Max Loss Point" is taken from the domain grid point with the maximum loss in SWE due to aerosol loading (located in the San Juan Range at 37.81N, -106.81W). The time series for "Relative Gain Point" was taken from the grid point downwind of "Max Loss Point" that represents the maximum local gain in SWE (37.35, -106.56), and "Near Neutral Point" is located along the ridge between the other two locations where the total change in SWE is near zero (37.32, -106.67).

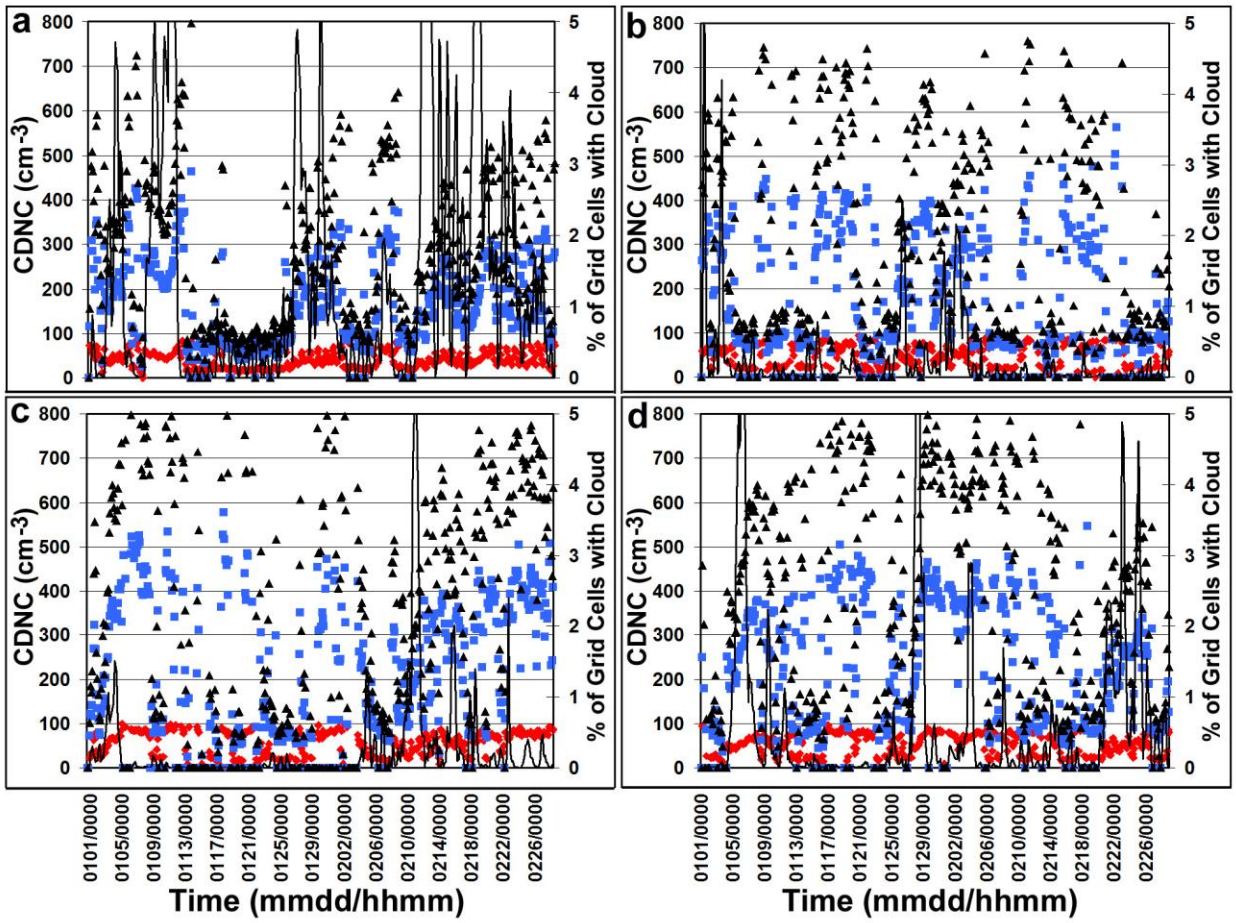

Figure 9. Cloud droplet number concentration (CDNC, cm^{-3}, markers) averaged over all cloudy grid cells every three hours for the duration of the 60-day simulations initialized with clean (red diamonds), polluted (blue squares), and highly polluted (black triangles) aerosol profiles. Also shown is the percent of domain grid cells containing cloud water of at least 0.05 g kg^{-1} (black contours) for the clean simulations. The panels are from the snow seasons of (a) 2005, (b) 2006, (c) 2007, and (d) 2008. CDNC is only averaged over grid cells with a cloud water content minimum of 0.05 g kg^{-1}.

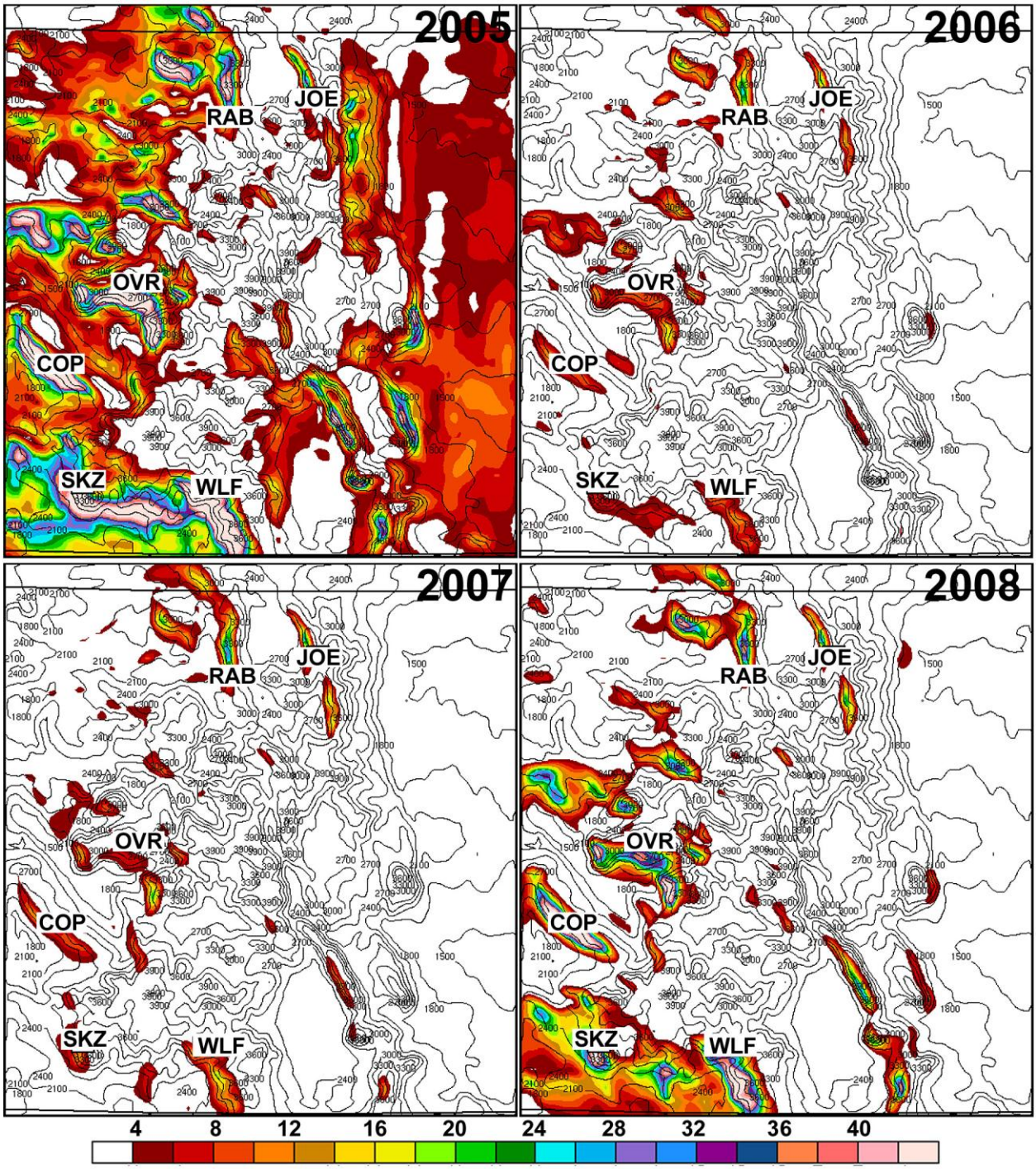

Figure 10. Mean cloud liquid water path (CWP) (mm x 1000) time averaged at 3-hourly intervals over 60 days on the 3km grid spacing domain. CWP is color shaded and topography (m) is contoured and labeled.

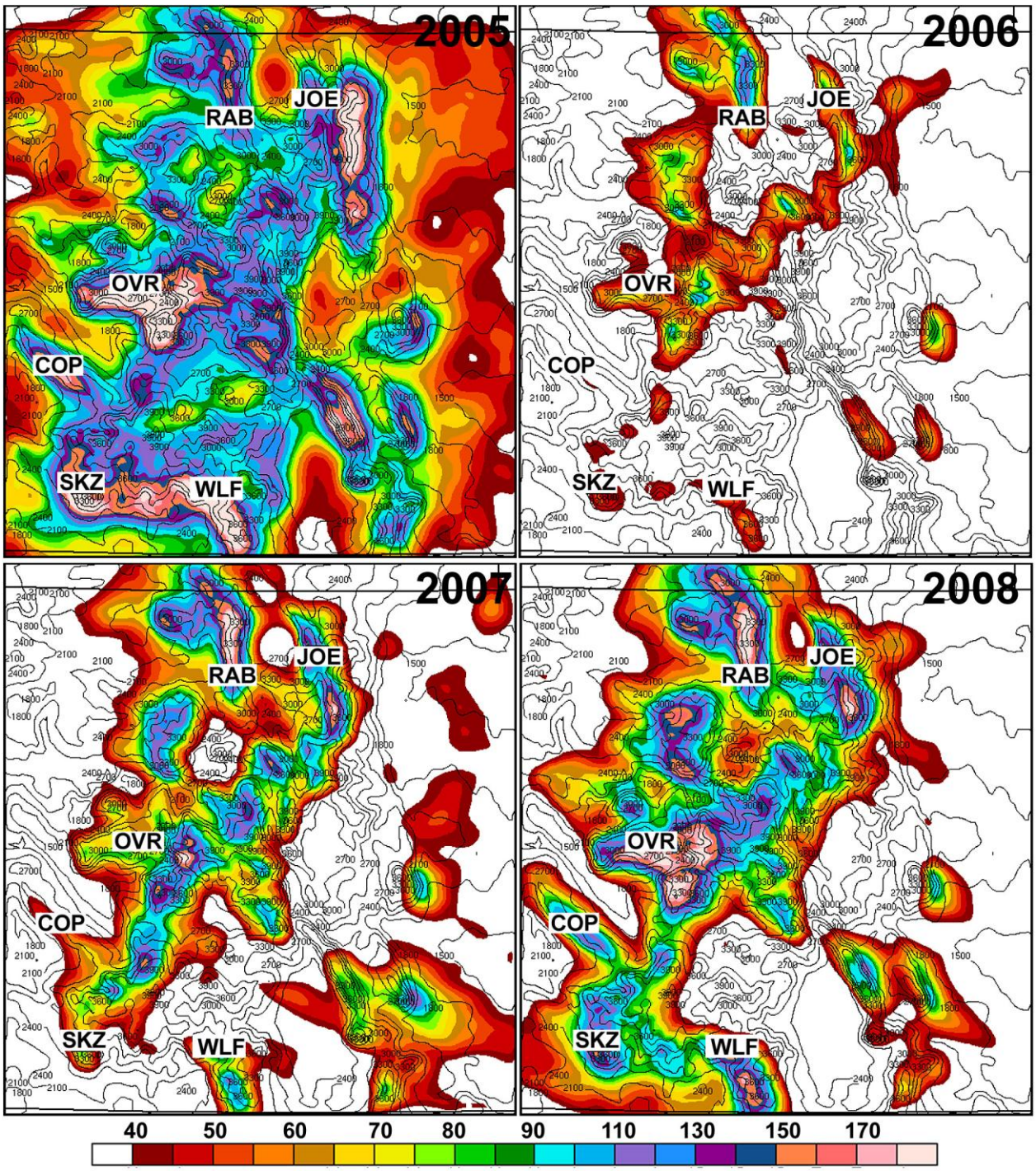

Figure 11. Mean ice water path (IWP) (mm x 1000) time averaged at 3-hourly intervals over 60 days on the 3km grid spacing domain. IWP is color shaded and topography (m) is contoured and labeled.

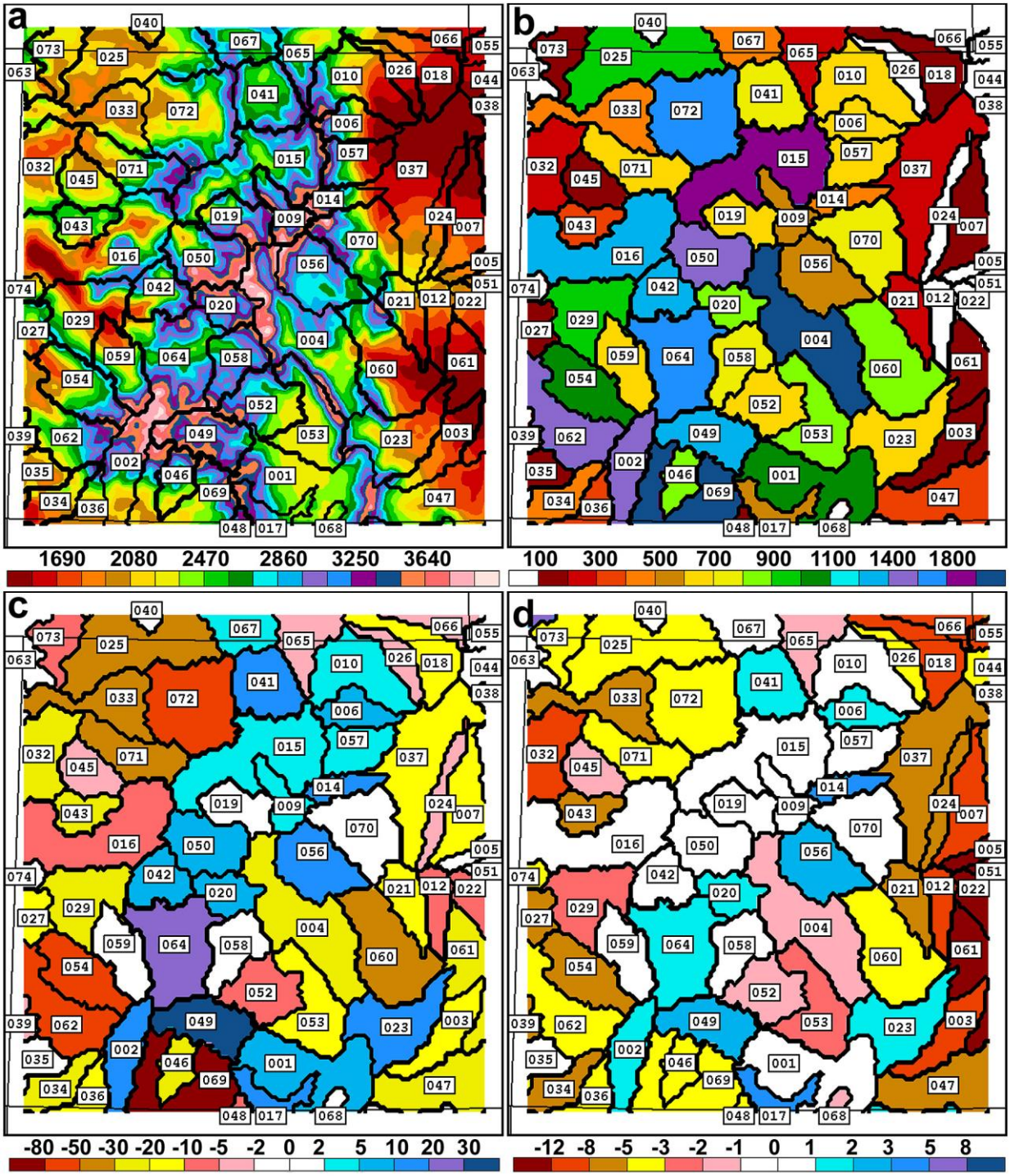

Figure 12. Simulated model variables divided into Colorado River Basins (outline in bold, black lines): (a) topography (m), (b) total accumulated basin volume precipitation (acre-feet / 1000) from the simulation with maximum aerosol concentration of 100 cm^{-3}, (c) change in basin volume precipitation (acre-feet / 1000) for an increase in maximum aerosol concentration from 100 to 1500 cm^{-3}, (d) same as (c) but given as % change. Basins are numbered according to Table 2.

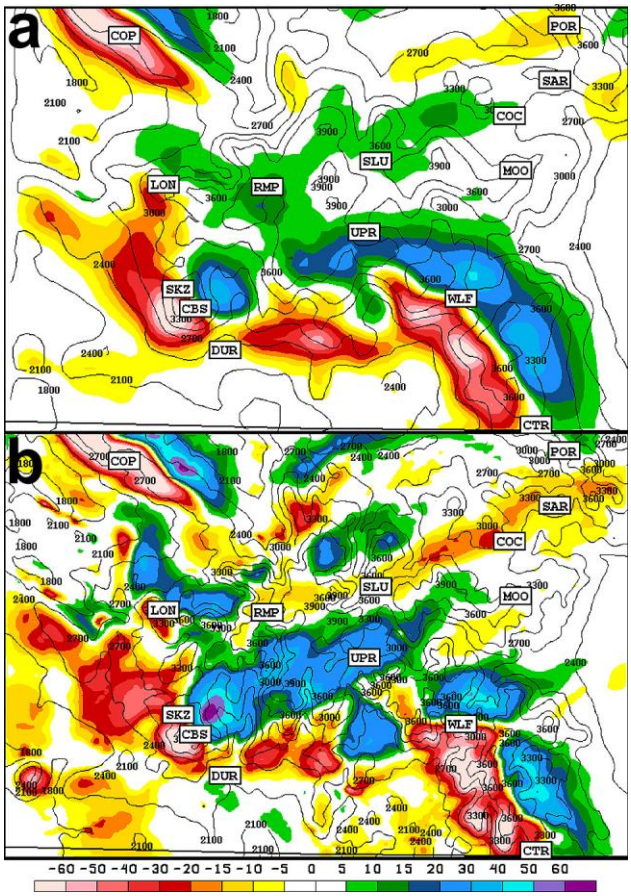

Figure 13. Difference in January 2005 accumulated (30-day) precipitation (mm) on the (a) 3-km and (b) 1-km grid spacing domains over Colorado between the highly polluted and clean simulations. Precipitation is color shaded and topography (m) is contoured and labeled. Negative (positive) values indicate a decrease (increase) in precipitation for an increase in aerosol concentration. The domain shown here covers the San Juan Range and is indicated by the rectangle partition in figure 7a.